

2'-Deoxyadenosine 5'-diphosphoribose is an endogenous TRPM2 superagonist

Running Head: 2'-Deoxy-ADPR is an endogenous superagonist of TRPM2

Ralf Fliegert¹, Andreas Bauche¹, Adriana-Michelle Wolf Pérez¹, Joanna M. Watt^{2,3}, Monika D. Rozewitz¹, Riekje Winzer¹, Mareike Janus¹, Feng Gu¹, Annette Rosche¹, Angelika Harneit¹, Marianne Flato¹, Christelle Moreau², Tanja Kirchberger¹, Valerie Wolters¹, Barry V.L. Potter^{2,3,*}, Andreas H. Guse^{1,*}

*equal contribution

¹The Calcium Signalling Group, Department of Biochemistry and Molecular Cell Biology, University Medical Centre Hamburg-Eppendorf, Martinistrasse 52, 20246 Hamburg, Germany

²Wolfson Laboratory of Medicinal Chemistry, Department of Pharmacy and Pharmacology, University of Bath, Bath, BA2 7AY, UK

³Medicinal Chemistry & Drug Discovery, Department of Pharmacology, University of Oxford, Mansfield Road, Oxford, OX1 3QT, UK

Abstract

Transient receptor potential melastatin 2 (TRPM2), is a ligand-gated Ca²⁺-permeable non-selective cation channel. While physiological stimuli, e.g. chemotactic agents, evoke controlled Ca²⁺ signals via TRPM2, pathophysiological signals, such as reactive oxygen species or genotoxic stress result in prolonged TRPM2-mediated Ca²⁺ entry and consequently apoptosis. To date, adenosine 5'-diphosphoribose (ADPR, **1**) has been assumed to be the main agonist for TRPM2. Here, we show that 2'-deoxy-ADPR **2** was a significantly better TRPM2

agonist, inducing 10.4-fold higher whole cell currents at saturation. Mechanistically, this increased activity was caused by decreased rate of inactivation and higher average open probability. Using high performance liquid chromatography (HPLC) and mass spectrometry, endogenous 2'-deoxy-ADPR was detected in Jurkat T-lymphocytes. Consistently, cytosolic nicotinamide mononucleotide adenylyltransferase 2 (NMNAT-2) and nicotinamide adenine dinucleotide (NAD)-glycohydrolase CD38 sequentially catalyzed synthesis of 2'-deoxy-ADPR from nicotinamide mononucleotide and 2'-deoxy-ATP *in vitro*. Thus, 2'-deoxy-ADPR is an endogenous TRPM2 superagonist that may act as cell signaling molecule.

32

33 **Introduction**

The C-terminal domain of TRPM2 is homologous to ADPR pyrophosphatase NUDT9. This discovery resulted in the identification of adenosine 5'-diphosphoribose (ADPR, **1**) as its agonist¹. An increase in cellular ADPR to activate TRPM2 is thought to proceed by hydrolysis of β -NAD either by NAD-glycohydrolase CD38 or via concerted action of poly-ADPR polymerases (PARPs) and poly-ADPR glycohydrolase (PARG) (reviewed in ²). The half maximal effective concentration (EC₅₀) for activation of TRPM2 by ADPR (reviewed in ³) implies that a significant amount of cellular NAD must be converted to ADPR to achieve activation. While this may make sense for the induction of apoptosis or cell death^{4,5}, it appears rather unlikely to be the case for physiological activation of TRPM2, e.g. in chemotaxis⁶, insulin secretion⁷, or thermosensation^{8,9}. Alternative activation mechanisms have been described, including direct activation by hydrogen peroxide¹⁰, by intracellular Ca²⁺ ions¹¹ or by *O*-acetyl-ADPR¹².

In summary, we show that among various ADPR analogues only 2'-deoxy-ADPR **2**, 3'-deoxy-ADPR **17**, 2'-phospho-ADPR **15**, and 2-F-ADPR **13** activated TRPM2. 2'-Deoxy-ADPR **2**

48 activated TRPM2 with similar potency but higher efficacy than ADPR, making 2'-deoxy-
49 ADPR a TRPM2 superagonist. The massive increase in macroscopic current induced by 2'-
50 deoxy-ADPR was due to decelerated TRPM2 inactivation and a higher average open
51 probability, while the single channel conductance remained unaffected. Further, we
52 demonstrate formation of 2'-deoxy-ADPR *in vitro* in two steps: from NMN and 2'-deoxy-
53 ATP to 2'-deoxy-NAD as catalyzed by NMNAT-2, and from 2'-deoxy-NAD to 2'-deoxy-
54 ADPR catalyzed by CD38. Finally, we proved the presence of endogenous 2'-deoxy-ADPR
55 and 2'-deoxy-NAD and present evidence for hydrogen peroxide-evoked increase of 2'-deoxy-
56 ADPR in Jurkat T cells. Importantly, 2'-deoxy-ADPR is not only a significantly better agonist
57 regarding TRPM2 activation than ADPR, but in addition does not require any NAD
58 consumption for its synthesis. 2'-deoxy-ADPR thus exhibits many of the properties expected
59 of a second messenger.

60

61 **Results**

62 *2'-Deoxy-ADPR as a TRPM2 superagonist*

63 Our interest in 2'-deoxy-ADPR as a potential TRPM2 agonist began when we probed the
64 structural requirements for activation of the channel. We assessed the agonist activity of
65 ADPR analogues (Supplementary Results, Supplementary Fig. 1–4) we had previously
66 evaluated as potential TRPM2 inhibitors¹³. These analogues feature modifications in the
67 purine base, the adenosine ribose, the pyrophosphate group and the terminal ribose. Published
68 EC₅₀ values for the activation of TRPM2 by ADPR are in the micromolar range (between
69 1 $\mu\text{mol/L}$ and 90 $\mu\text{mol/L}$)³ indicating an interaction of rather low affinity. We therefore
70 anticipated that many of the analogues might activate TRPM2. To our surprise most of the
71 analogues had no, or negligible, agonist activity (Fig. 1). Among the ADPR analogues with

72 modifications at the purine ring only 2-F-ADPR retained partial agonist activity (Fig. 1).
73 These results clearly demonstrate the requirement of a combination of terminal ribose,
74 pyrophosphate, and adenosine motifs for activation of TRPM2.

75 The part of ADPR most permissive to modifications was the adenosine ribose. 2'-Phospho-
76 ADPR showed partial agonist activity albeit at higher concentrations (EC_{50} 110 μ mol/L) and
77 with reduced efficacy ($0.56 \text{ nA} \pm 0.64 \text{ nA}$, best-fit value \pm standard error (SE)) compared to
78 ADPR ($1.60 \text{ nA} \pm 0.47 \text{ nA}$, best-fit value \pm SE) (Fig. 2a), in good agreement with a recent
79 study¹⁴. The most interesting finding, however, came from our attempt to establish the role of
80 the 2'- and 3'-hydroxyl groups of the adenosine ribose. While 3'-deoxy-ADPR showed an
81 EC_{50} comparable to that of ADPR (EC_{50} 46 μ mol/L and 28 μ mol/L, respectively) and elicited
82 only a slightly reduced maximum current ($1.23 \text{ nA} \pm 0.52 \text{ nA}$, best-fit value \pm SE), 2'-deoxy-
83 ADPR activated TRPM2 at somewhat lower concentrations than ADPR (Fig. 2a). Most
84 importantly, 2'-deoxy-ADPR induced 10.4-fold higher currents in the whole cell
85 configuration (Fig. 2a). Whole cell patch clamp experiments with the human T cell line Jurkat
86 that endogenously expresses TRPM2^{4,15-17} confirmed the induction of significantly higher
87 currents by 2'-deoxy-ADPR as compared to ADPR. In contrast to HEK293 cells, Jurkat cells
88 in the majority of experiments did not tolerate 2'-deoxy-ADPR concentrations $> 100 \mu$ mol/L,
89 likely due to the high Ca^{2+} and Na^{+} influx (Fig. 2b). Under physiological ionic conditions, in
90 these experiments the I-V curve obtained from voltage ramps was nearly linear and was
91 characterized by a reversal potential near 0 (Supplementary Fig. 5b), regardless of the
92 activating agonist. These results clearly demonstrate that 2'-deoxy-ADPR is a TRPM2
93 superagonist.

94 The increase in whole cell current after activation by superagonists might be explained either
95 by the preferential occupation of higher conductance states, as has been shown for the
96 insecticide clothianidin, a superagonist of the nicotinic acetylcholine receptor¹⁸, by induction

of an otherwise inaccessible higher conductance state, or by a change in kinetics allowing the channel to remain in the open state for longer periods of time, as is the case for 4,5,6,7-tetrahydroisoxazolo[5,4-*c*]pyridin-3(2*H*)-one (THIP), a superagonist of the $\alpha_4\beta_3\delta$ GABA receptor¹⁹. To distinguish between these possibilities we performed recordings on excised inside/out patches from cells expressing either wild type hTRPM2 (Fig 3a+b+c) or hTRPM2 with modified selectivity filter (T5L) that shows increased affinity to permeating cations resulting in higher single channel conductivity²⁰. The results showed no significant difference in single channel conductance (Fig. 3c) upon activation by either ADPR or 2'-deoxy-ADPR. Instead, the inactivation of TRPM2 following 2'-deoxy-ADPR activation was significantly slower compared to ADPR (Fig 3d+e+f; 2'-deoxy ADPR: $0.050\text{ s}^{-1} \pm 0.003\text{ s}^{-1}$ vs ADPR: $0.037\text{ s}^{-1} \pm 0.003\text{ s}^{-1}$, best-fit values \pm SE, extra sum-of-squares F test, $p=0.001$). Further, the average open probability was 37% higher (Fig. 3d+g) for activation by 2'-deoxy-ADPR (median 0.92, interquartile range (IQR) 0.80 to 0.97) compared to ADPR (median 0.67, IQR 0.17 to 0.74, Mann-Whitney test, $p<0.0001$). In addition, we also observed an approx. 5-fold increase in the number of channels simultaneously in the open state when excised patches were exposed to 2'-deoxy-ADPR (Fig. 3d+h), at least partially attributable to the increased open probability. Whole cell patch clamp experiments with different Ca^{2+} concentrations in the pipette buffer solution demonstrated a reduced Ca^{2+} -sensitivity of activation of TRPM2 by 2'-deoxy-ADPR when compared to activation by ADPR (Fig. 2c). Whereas the maximum current induced by ADPR (as obtained from the concentration-response curve) increased by 140% (from $0.67\text{ nA} \pm 1.07\text{ nA}$ to $1.60\text{ nA} \pm 0.47\text{ nA}$) when the free $[\text{Ca}^{2+}]$ was raised from 50 nmol/L to 200 nmol/L, the maximum current induced by 2'-deoxy-ADPR increased only by 16% (from $14.3\text{ nA} \pm 1.45\text{ nA}$ to $16.7\text{ nA} \pm 0.74\text{ nA}$, best-fit values \pm SE). At (supraphysiological) saturating concentrations for Ca^{2+} and ADPR the open probability of human TRPM2 approaches a value of one²¹. It therefore seems likely that in intact cells

activation by 2'-deoxy-ADPR is less sensitive to Ca^{2+} , with the concentration-response for Ca^{2+} shifted to the left, allowing for higher open probabilities and larger whole cell currents at physiological Ca^{2+} concentrations.

Biosynthetic pathways for 2'-deoxy-ADPR

Superagonist behavior has previously been observed with pharmacological modulators of ligand-gated ion channels usually having little or no resemblance to the natural ligands. However, 2'-deoxy-ADPR is closely related to ADPR. Thus, we hypothesized that 2'-deoxy-ADPR might be an endogenous modulator of TRPM2.

A conceivable endogenous pathway to 2'-deoxy-ADPR would be the hydrolysis of 2'-deoxy-NAD by either CD38 or the PARP/PARG system. 2'-Deoxy-NAD can be synthesized by nicotinamide mononucleotide adenylyltransferase (NMNAT, EC 2.7.7.1) catalyzing the condensation of β -nicotinamide mononucleotide (NMN) and 2'-deoxy-ATP, as has been shown for NMNAT from yeast²² and human NMNAT-1²³. There are three different isoforms of NMNAT with distinct subcellular localization that contribute to different NAD pools²⁴. Here we demonstrate for the first time that NMNAT-2, the isoform that presumably maintains the cytoplasmic NAD pool²⁴, also catalyzed the conversion of 2'-deoxy-ATP and NMN to 2'-deoxy-NAD (Fig. 4a; Supplementary Fig. 6). At a saturating concentration of 500 $\mu\text{mol/L}$ β -NMN the $K_{0.5}$ for 2'-deoxy-ATP is $3.28 \text{ mmol/L} \pm 0.55 \text{ mmol/L}$ (Michaelis-Menten constant K_M for ATP $611 \text{ } \mu\text{mol/L} \pm 31 \text{ } \mu\text{mol/L}$, both best-fit values \pm SE). Interestingly, the enzyme did not only show cooperativity (Hill coefficient n_H 1.4 ± 0.1 , best-fit value \pm SE) with regard to 2'-deoxy ATP, but was also inhibited by high concentrations of the substrate, which is clearly not the case for ATP (Fig. 4b).

Next we explored potential pathways for generation of 2'-deoxy-ADPR via both the PARP/PARG and CD38 pathways. Since it was shown in isolated nuclei that 2'-deoxy-ADPR

was incorporated into poly-ADPR polymers of nuclear proteins²⁵, we analyzed whether poly-ADP ribosylated proteins actually contain 2'-deoxy-ADPR residues. Poly-ADP-ribosylated proteins were isolated from HEK293 cells previously exposed to H₂O₂^{5,26}. An increase of the amount of poly-ADP ribosylated proteins, compared to unstimulated controls was confirmed by western blot analysis (Supplementary Fig. 7, upper inset). The immunoprecipitate was then hydrolyzed by recombinant human PARG. Analysis of products by HPLC showed significant amounts of ADPR and a small amount of AMP, most likely due to spontaneous degradation of ADPR (Supplementary Fig. 7, central panel), but despite the high sensitivity of the method (40 fmol at signal-to-noise (S/N) ratio ≥ 3) no 2'-deoxy-ADPR was detected (Supplementary Fig. 7, central and lower panel). Thus, it is unlikely that release of 2'-deoxy-ADPR from poly-ADP-ribosylated proteins by PARG significantly contributes to TRPM2 activation.

Next we tested whether CD38 might produce 2'-deoxy-ADPR. CD38 is well known to be expressed as ecto-enzyme (type II orientation), but recently evidence for type III orientation with the active site facing the cytoplasm was presented²⁷, thereby potentially allowing turnover of cytosolic 2'-deoxy-NAD. Recombinant soluble human CD38 completely hydrolyzed 2'-deoxy-NAD to a product that co-eluted with chemically synthesized 2'-deoxy-ADPR (Fig. 4c). Product identity was confirmed by spiking with authentic 2'-deoxy-ADPR (Supplementary Fig. 8a) and hydrolysis by pyrophosphatase to 2'-deoxy-AMP (Supplementary Fig. 8b). Further, type III CD38 enzyme activity, though small in comparison to ecto-enzyme (type II) CD38 enzyme activity, was clearly detected in Jurkat T cells (Fig. 4d). While in CD38^{-/-} cells measurable NAD glycohydrolase was not detected (Fig. 4d, left), specific inhibition of ecto-CD38 by 2'-deoxy-2'-fluoro arabinosyl NAD (araF-NAD)²⁸, forming a stable covalent inhibitor-CD38 complex, almost completely abolished type II CD38 activity (Fig. 4d, middle, 1st araF-NAD addition). Permeabilization of such cells with saponin allowed to access type III CD38 and to determine its activity (Fig. 4d, right). Specificity was

demonstrated by a 2nd addition of araF-NAD fully blocking type III CD38 (Fig. 4d, right). Kinetic analysis using NAD vs 2'-deoxy-NAD as substrates resulted in 9.2-fold higher affinity of CD38 for 2'-deoxy-NAD and comparable values for maximal velocity V_{\max} (Supplementary Fig. 8c). Collectively, strong evidence is presented that 2'-deoxy-NAD serves as a substrate for type III CD38 to produce 2'-deoxy-ADPR, while 2'-deoxy-NAD can be produced from the abundant cellular metabolites nicotinamide mononucleotide and 2'-deoxy-ATP by cytosolic NMNAT (Supplementary Fig. 9).

2'-Deoxy-ADPR and 2'-deoxy-NAD present in Jurkat cells

To detect endogenous 2'-deoxy-ADPR and 2'-deoxy-NAD in Jurkat T cells, we used two consecutive reversed phase (RP)-HPLC separations on C8 and C18 columns using a volatile ammonium acetate buffer to allow for subsequent high resolution mass spectrometry (Fig. 5a+b+c). Fractions pre-fractionated on a C8 column (Fig. 5a) and co-eluting with 2'-deoxy-ADPR and 2'-deoxy-NAD on a C18 column (Fig. 5b+c) showed molecular ions corresponding to 2'-deoxy-ADPR (observed mass $[M-H]^-$ 542.0722, calculated mass: 542.0695) and 2'-deoxy-NAD (observed mass $[M-H]^-$ 646.1104, calculated mass: 646.1069) (Supplementary Fig. 10 a+b). The main electrospray ionization (ESI) fragmentation products of 2'-deoxy-ADPR and 2'-deoxy-NAD, 2'-deoxy-AMP ($[M-H]^-$ 330.0633) and 2'-deoxy-ADP ($[M-H]^-$ 410.0304), were prominent in both samples. Since it is unlikely that both products co-eluted with 2'-deoxy-ADPR and 2'-deoxy-NAD during two-dimensional HPLC, these molecular ions are most likely to result from fragmentation of 2'-deoxy-ADPR and 2'-deoxy-NAD during mass spectrometry. The HPLC system based on ammonium acetate eluents was suitable for quantification of endogenous 2'-deoxy-NAD (Fig. 5c+g), amounting to 5.05 ± 0.58 pmol/ 10^7 cells (mean \pm SEM, n=12, significantly different from a theoretical median of 0, Wilcoxon Signed Rank Test). The concentration of 2'-deoxy-NAD was not significantly affected by exposure of the cells to hydrogen peroxide

(5.67 ± 0.78 pmol/ 10^7 cells, mean \pm SEM, n=11) (Fig. 5c+g). To investigate any role of CD38 in the synthesis of 2'-deoxy-ADPR in Jurkat T cells, CD38 was knocked-out using CRISPR (Clustered Regularly Interspaced Short Palindromic Repeats)/Cas9 technology^{29,30}. P10 membranes of the resulting CD38^{-/-} cell line did not show NAD glycohydrolase activity and were negative for CD38 in western blot analysis (Supplementary Fig 11). Neither was the endogenous concentration of 2'-deoxy-NAD significantly affected by knock-out of CD38 nor by hydrogen peroxide stimulation (Fig. 5 d+f+g). In addition, we also analyzed cellular ADPR and NAD contents under these conditions (Supplementary Fig 12). As expected, NAD was present in much higher quantities (7.58 ± 0.42 nmol/ 10^7 cells, mean \pm SEM, n=12), but was not affected by knockout of NAD glycohydrolase CD38 (6.42 ± 0.30 nmol/ 10^7 cells, mean \pm SEM, n=15). Exposure to hydrogen peroxide did, at least during the 5 min of the experiment, not affect NAD (p=0.78 for wild type and p=0.62 for CD38^{-/-} cells). ADPR was found in quantities (292 ± 79 pmol/ 10^7 cells, mean \pm SEM, n=11) consistent with our previous results⁴, but was neither significantly affected by knockout of CD38 nor by exposure to hydrogen peroxide.

In contrast to almost baseline-separated 2'-deoxy-NAD (Fig. 5c+f), HPLC using volatile ammonium acetate buffer (ideally suited for subsequent mass spectrometry) did not allow for baseline separation of 2'-deoxy-ADPR (Fig. 5b+e). Though 2'-deoxy-ADPR was qualitatively identified (i) by its retention time, (ii) by using samples from cell extracts spiked with a small amount of authentic 2'-deoxy-ADPR (Fig. 5b+e), and (iii) by mass spectrometry (Supplementary Fig. 10a), the separation on a C18 column was not sufficient to quantify 2'-deoxy-ADPR reliably (Fig. 5b+e). However, we noted that the peak containing 2'-deoxy-ADPR increased after stimulation with hydrogen peroxide. Further, comparison of the chromatograms of samples from wildtype (Fig. 5b) and CD38^{-/-} cells (Fig. 5e) shows that the peak containing 2'-deoxy-ADPR was absent in the samples from CD38^{-/-} cells regardless of

whether they have been exposed to H₂O₂ or not, suggesting that 2'-deoxy-ADPR is produced from 2'-deoxy-NAD by CD38.

Using ion-pair instead of conventional RP-HPLC, two consecutive separations on C8 and C18 columns (Fig. 6) resulted in sufficient separation of endogenous 2'-deoxy-ADPR for quantification (Fig. 6a, lower panel). Here, 2'-deoxy-ADPR was identified using authentic 2'-deoxy-ADPR as standard or in a spiked sample (Fig 6a). Recovery of 2'-deoxy-ADPR was determined using 1, *N*⁶-etheno-adenosine (Supplementary Fig 13). Any trials to identify 2'-deoxy-ADPR by mass spectrometry in this HPLC system failed due to the presence of the ion pair reagent in the collected samples; furthermore, several procedures tested to deplete the ion pair reagent were not successful. However, using this ion-pair RP-HPLC separations on C8 and C18 columns, 2'-deoxy-ADPR was detected in Jurkat cells and determined to be 35 pmol/10⁷ cells (median, interquartile range (IQR): 17 pmol/10⁷ cells to 50 pmol/10⁷ cells, significantly different from a theoretical median of 0, Wilcoxon Signed Rank Test). As hydrogen peroxide treatment results in TRPM2 activation, we then tested the impact of H₂O₂ on the endogenous 2'-deoxy-ADPR concentration (Fig. 6b+c). After 5 min the amount of 2'-deoxy-ADPR rose significantly by 2.71 fold to 95 pmol/10⁷ cells (median, IQR: 42 pmol/10⁷ cells to 116 pmol/10⁷ cells).

Discussion

It is widely accepted that TRPM2 can be activated downstream of reactive oxygen species like hydrogen peroxide^{10,31}. Despite reports of direct activation of the channel by hydrogen peroxide³², this has mostly been attributed to the generation of ADPR by the consecutive action of PARP and PARG^{5,33}. Especially during certain cell cycle phases, 2'-deoxy-ADPR as an additional mechanism might contribute to this process: hydrogen peroxide-induced DNA damage can cause a replication arrest during S phase, which would result in an accumulation

of 2'-deoxy-ATP, because deoxy-nucleoside triphosphates will no longer be consumed by the replication machinery. In addition, the activation of PARPs following DNA damage will result in consumption of NAD for poly-ADP ribosylation. The consequent drop in cellular NAD will increase its synthesis, which ultimately results in decreased cellular ATP pools. The increased ratio of 2'-deoxy-ATP to ATP then facilitates synthesis of 2'-deoxy-NAD by NMNAT and subsequent hydrolysis to 2'-deoxy-ADPR by CD38. The latter reaction is preferred due to the 9.2-fold higher affinity of CD38 for 2'-deoxy-NAD, as compared to NAD (see Supplementary Fig. 8c). The increase in cellular 2'-deoxy-ADPR then either mediates TRPM2 activation on its own or contributes to TRPM2 activation mediated by ADPR derived from PARP/PARG activity.

How do the nucleotide determinations from cell extracts translate into cytosolic, or even sub-plasmalemmal, concentrations? Assuming a mean diameter of Jurkat cells of $11.5\ \mu\text{m}$ ³⁴, a cellular 2'-deoxy-ADPR concentration of $4.4\ \mu\text{mol/L}$ can be calculated. However, the lymphocyte is not simply a sphere filled with aqueous liquid, but contains solid material, e.g. organelles, DNA, proteins. This solid portion is difficult to calculate, but well known for Jurkat cells is the nucleus volume, amounting to 55% of the total volume³⁴. Using this portion to distinguish the cytosolic from the intra-nuclear space, the cytosolic concentration of 2'-deoxy-ADPR amounts to $9.8\ \mu\text{mol/L}$, a value found in the lower part of the concentration-response curve (Fig. 2). Upon stimulation by hydrogen peroxide this cytosolic concentration within 5 min rises to $26.6\ \mu\text{mol/L}$. If we further assume that the concentration of 2'-deoxy-ADPR in the cytosol is not evenly distributed, but is increased at the site of its biosynthesis, the sub-plasmalemmal space where the catalytic center of type III CD38 is localized²⁷, then the local concentrations are readily in the dynamic range of the concentrations response curve(s) shown in Fig. 2, especially at slightly elevated free cytosolic Ca^{2+} concentrations, e.g. $200\ \text{nM}$ (Fig. 2c). Besides 2'-deoxy-ADPR, we also established the presence of

endogenous 2'-deoxy-NAD, the potential precursor of 2'-deoxy-ADPR. The cytosolic concentration of 2'-deoxy-NAD is low at 1.41 $\mu\text{mol/L}$, in comparison to the cellular concentration of NAD (955 $\mu\text{mol/L}$). This indicates that 2'-deoxy-NAD represents a nucleotide with specialized function(s), very much in contrast to NAD that serves as (co)-substrate for a plethora of enzymatic reactions. The kinetic parameters obtained for NMNAT-2 (Fig. 2c) suggest that inside the cell mainly ATP is used to maintain the cellular NAD pool. However, upon stimulation with hydrogen peroxide, small amounts of 2'-deoxy-ATP appear to flux via 2'-deoxy-NAD into 2'-deoxy-ADPR; substrate inhibition of NMNAT-2 by 2'-deoxy-ATP, but not ATP, indicates that the pathway towards 2'-deoxy-ADPR is a highly regulated process. It has not escaped our notice that the presence of endogenous 2'-deoxy-NAD also in principle presents the possibility for generation of 2'-deoxy-cADPR by CD38, in addition to 2'-deoxy ADPR. While 2'-deoxy-cADPR was shown to be equipotent to cADPR in Ca^{2+} signaling in sea urchin³⁵, like its 3'-deoxy congener, it was not active in Jurkat T cells³⁶ excluding the need to consider 2'-deoxy-cADPR more widely in a signaling context.

Our results might solve an important conceptual problem concerning activation of TRPM2: Cellular NAD serves many functions, most prominently as redox coenzyme, as co-substrate for sirtuins, and as precursor for nicotinamide adenine dinucleotide phosphate (NADP) and the second messengers cyclic adenosine diphosphoribose (cADPR) and nicotinic acid adenine dinucleotide phosphate (NAADP, reviewed in²⁴). NAD depletion appears therefore incompatible with life and has been shown to ultimately result in cell death³⁷. We therefore consider it unlikely that during physiological activation the amount of ADPR necessary for TRPM2 activation, especially at resting Ca^{2+} concentrations, is generated by turnover of nuclear, cytosolic or mitochondrial NAD pools. In contrast, a small cytosolic pool of 2'-deoxy-NAD might be maintained, for instance by NMNAT, independently of NAD, since 2'-deoxy-NAD can neither be phosphorylated by NAD kinase to yield 2'-deoxy-NADP nor is it a

good substrate for NAD dependent dehydrogenases^{22,38,39}. Thus, formation of 2'-deoxy-ADPR from 2'-deoxy-NAD by type III CD38 does not interfere with energy metabolism and other NAD functions. Previous work demonstrating that CD38 hydrolyzed 2'-deoxy-NAD with similar V_{max} as NAD⁴⁰ is confirmed here; however, a 9.2-fold higher affinity for 2'-deoxy-NAD as compared to NAD was determined (Supplementary Fig. 8c). Thus, we present here a possible mechanism for the generation of 2'-deoxy-ADPR via conversion of cytosolic 2'-deoxy-NAD by CD38 in a type III orientation. However, since the endogenous concentration of 2'-deoxy-NAD is small and the relative activity of CD38 in the type III orientation that we observed was low, generation of 2'-deoxy-ADPR may be accomplished via alternative pathways.

Taken together, we demonstrate that 2'-deoxy-ADPR is the most efficient endogenous agonist of TRPM2 described to date. In addition, 2'-deoxy-ADPR appears to be the first superagonist for an ion channel that can be synthesized by the enzymatic machinery of most cell types. Our results suggest the possibility that TRPM2 can be activated in context-specific manner. In pathological cell death in neurodegenerative diseases⁴¹, stroke⁴², or myocardial infarction⁴³, ADPR may be generated by PARP/PARG³³ or by CD38 thereby not only triggering TRPM2 activation, but also depleting cellular NAD and ATP pools. In contrast, since physiological processes, e.g. neutrophil chemotaxis, require an intact cytoplasmic NAD pool, 2'-deoxy-ADPR may activate TRPM2 without consumption of NAD, thus acting independently of energy metabolism. Taken together, the confluence of properties associated with 2'-deoxy-ADPR may point to a physiological role for the molecule as a novel second messenger activating TRPM2.

Acknowledgements

This study was supported by the Deutsche Forschungsgemeinschaft (GU 360/16-1 to AHG), the Wellcome Trust (Project Grant 084068 to BVLP and AHG and Programme Grant 082837 to BVLP), and Landesforschungsförderung Hamburg (Research Group ReAd Me to AHG). BVLP is a Wellcome Trust Senior Investigator (Grant 101010).

Author contributions

AHG, BVLP and RF designed the study and individual experiments. CM and JMW synthesized and purified the ADPR analogues. TK, RF and MDR performed electrophysiological characterization of ADPR analogues. MDR carried out the single channel recordings. AMWP and AB performed the enzyme assays with NMNAT and CD38. RW analyzed nucleotide products from poly ADP-ribosylated proteins. RF and AH prepared TRPM2 T5L and CD38 expression vectors and generated the TRPM2 T5L cell line. AB, AWMP and MJ established the HPLC method for determination of endogenous 2'-deoxy-ADPR. AB and MJ quantitatively analyzed endogenous nucleotides. AB determined substrate saturation plots for NMNAT-2 and sCD38. JMW performed the HRMS analysis of 2'-deoxy-ADPR and 2'-deoxy-NAD. VW generated the CD38^{-/-} Jurkat cell line and produced and purified soluble recombinant CD38. MF characterized the CD38^{-/-} Jurkat cell line. AR, AB and FG determined the activity of CD38 in type III orientation. All authors wrote the manuscript.

References for main text

1. Perraud, A. L. *et al.* ADP-ribose gating of the calcium-permeable LTRPC2 channel

- revealed by Nudix motif homology. *Nature* **411**, 595–599 (2001).
2. Knowles, H., Li, Y. & Perraud, A. L. The TRPM2 ion channel, an oxidative stress and metabolic sensor regulating innate immunity and inflammation. *Immunol. Res.* **55**, 241–248 (2013).
3. Faouzi, M. & Penner, R. in *Mammalian Transient Receptor Potential (TRP) Cation Channels* (eds. Dietrich, A. & Gudermann, T.) **222**, 157–188 (2014).
4. Gasser, A. *et al.* Activation of T cell calcium influx by the second messenger ADP-ribose. *J. Biol. Chem.* **281**, 2489–2496 (2006).
5. Buelow, B., Song, Y. & Scharenberg, A. M. The Poly(ADP-ribose) polymerase PARP-1 is required for oxidative stress-induced TRPM2 activation in lymphocytes. *J. Biol. Chem.* **283**, 24571–24583 (2008).
6. Partida-Sanchez, S. *et al.* Chemotaxis of mouse bone marrow neutrophils and dendritic cells is controlled by adp-ribose, the major product generated by the CD38 enzyme reaction. *J. Immunol.* **179**, 7827–7839 (2007).
7. Uchida, K. *et al.* Lack of TRPM2 impaired insulin secretion and glucose metabolisms in mice. *Diabetes* **60**, 119–126 (2011).
8. Song, K. *et al.* The TRPM2 channel is a hypothalamic heat sensor that limits fever and can drive hypothermia. *Science* **353**, 1393–1398 (2016).
9. Tan, C.-H. & McNaughton, P. A. The TRPM2 ion channel is required for sensitivity to warmth. *Nature* **536**, 460–3 (2016).
10. Wehage, E. *et al.* Activation of the cation channel long transient receptor potential channel 2 (LTRPC2) by hydrogen peroxide: A splice variant reveals a mode of activation independent of ADP-ribose. *J. Biol. Chem.* **277**, 23150–23156 (2002).

- 365 11. Du, J., Xie, J. & Yue, L. Intracellular calcium activates TRPM2 and its alternative
366 spliced isoforms. *Proc. Natl. Acad. Sci. U. S. A.* **106**, 7239–7244 (2009).
- 367 12. Grubisha, O. *et al.* Metabolite of SIR2 reaction modulates TRPM2 ion channel. *J. Biol.*
368 *Chem.* **281**, 14057–14065 (2006).
- 369 13. Moreau, C. *et al.* Structure-activity relationship of adenosine 5'-diphosphoribose at the
370 transient receptor potential melastatin 2 (TRPM2) channel: Rational design of
371 antagonists. *J. Med. Chem.* **56**, 10079–10102 (2013).
- 372 14. Tóth, B., Iordanov, I. & Csanády, L. Ruling out pyridine dinucleotides as true TRPM2
373 channel activators reveals novel direct agonist ADP-ribose-2'-phosphate. *J. Gen.*
374 *Physiol.* **145**, 419–430 (2015).
- 375 15. Sano, Y. *et al.* Immunocyte Ca²⁺ influx system mediated by LTRPC2. *Science* **293**,
376 1327–1330 (2001).
- 377 16. Beck, A., Kolisek, M., Bagley, L. A., Fleig, A. & Penner, R. Nicotinic acid adenine
378 dinucleotide phosphate and cyclic ADP-ribose regulate TRPM2 channels in T
379 lymphocytes. *FASEB J.* **20**, 962–4 (2006).
- 380 17. Klumpp, D. *et al.* Targeting TRPM2 Channels Impairs Radiation-Induced Cell Cycle
381 Arrest and Fosters Cell Death of T Cell Leukemia Cells in a Bcl-2-Dependent Manner.
382 *Oxid. Med. Cell. Longev.* **2016**, 8026702 (2016).
- 383 18. Brown, L. A., Ihara, M., Buckingham, S. D., Matsuda, K. & Sattelle, D. B.
384 Neonicotinoid insecticides display partial and super agonist actions on native insect
385 nicotinic acetylcholine receptors. *J. Neurochem.* **99**, 608–615 (2006).
- 386 19. Mortensen, M., Ebert, B., Wafford, K. & Smart, T. G. Distinct activities of GABA
387 agonists at synaptic- and extrasynaptic-type GABAA receptors. *J. Physiol.* **588**, 1251–

- 388 1268 (2010).
- 389 20. Tóth, B. & Csanády, L. Pore collapse underlies irreversible inactivation of TRPM2
390 cation channel currents. *Proc. Natl. Acad. Sci. U. S. A.* **109**, 13440–13445 (2012).
- 391 21. Csanády, L. & Töröcsik, B. Four Ca²⁺ ions activate TRPM2 channels by binding in
392 deep crevices near the pore but intracellularly of the gate. *J. Gen. Physiol.* **133**, 189–
393 203 (2009).
- 394 22. Klenow, H. & Andersen, B. Some enzyme reactions with adenine deoxyriboside
395 polyphosphates. *Biochim. Biophys. Acta* **23**, 92–97 (1957).
- 396 23. Emanuelli, M. *et al.* Molecular cloning, chromosomal localization, tissue mRNA
397 levels, bacterial expression, and enzymatic properties of human NMN
398 adenylyltransferase. *J. Biol. Chem.* **276**, 406–412 (2001).
- 399 24. Di Stefano, M. & Conforti, L. Diversification of NAD biological role: the importance
400 of location. *FEBS J.* **280**, 4711–28 (2013).
- 401 25. Suhadolnik, R. J. *et al.* ADP-Ribosylation of Isolated Nuclei from HeLa Cells, Rat
402 Liver , Fetal Rat Liver , and Novikoff Rat Hepatoma. *J. Biol. Chem.* **252**, 4134–4144
403 (1977).
- 404 26. Bakondi, E. *et al.* Detection of poly(ADP-ribose) polymerase activation in oxidatively
405 stressed cells and tissues using biotinylated NAD substrate. *J. Histochem. Cytochem.*
406 **50**, 91–8 (2002).
- 407 27. Zhao, Y. J., Lam, C. M. C. & Lee, H. C. The Membrane-Bound Enzyme CD38 Exists
408 in Two Opposing Orientations. *Sci. Signal.* **5**, ra67-ra67 (2012).
- 409 28. Muller-Steffner, H. M., Malver, O., Hosie, L., Oppenheimer, N. J. & Schuber, F. Slow-
410 binding inhibition of NAD⁺ glycohydrolase by arabino analogues of beta-NAD. *J.*
-

- 411 *Biol. Chem.* **267**, 9606–11 (1992).
- 412 29. Mali, P. *et al.* RNA-guided human genome engineering via Cas9. *Science* **339**, 823–6
413 (2013).
- 414 30. Cong, L. *et al.* Multiplex genome engineering using CRISPR/Cas systems. *Science*
415 **339**, 819–23 (2013).
- 416 31. Hara, Y. *et al.* LTRPC2 Ca²⁺-permeable channel activated by changes in redox status
417 confers susceptibility to cell death. *Mol. Cell* **9**, 163–73 (2002).
- 418 32. Heiner, I. *et al.* Expression profile of the transient receptor potential (TRP) family in
419 neutrophil granulocytes: evidence for currents through long TRP channel 2 induced by
420 ADP-ribose and NAD. *Biochem. J.* **371**, 1045–53 (2003).
- 421 33. Fonfria, E. *et al.* TRPM2 channel opening in response to oxidative stress is dependent
422 on activation of poly(ADP-ribose) polymerase. *Br. J. Pharmacol.* **143**, 186–192
423 (2004).
- 424 34. Rosenbluth, M. J., Lam, W. A. & Fletcher, D. A. Force microscopy of nonadherent
425 cells: a comparison of leukemia cell deformability. *Biophys. J.* **90**, 2994–3003 (2006).
- 426 35. Ashamu, G. A., Sethi, J. K., Galione, A. & Potter, B. V. Roles for adenosine ribose
427 hydroxyl groups in cyclic adenosine 5'-diphosphate ribose-mediated Ca²⁺ release.
428 *Biochemistry* **36**, 9509–17 (1997).
- 429 36. Moreau, C. *et al.* Synthesis of cyclic adenosine 5'-diphosphate ribose analogues: a
430 C2'endo/syn 'southern' ribose conformation underlies activity at the sea urchin cADPR
431 receptor. *Org. Biomol. Chem.* **9**, 278–90 (2011).
- 432 37. Del Nagro, C., Xiao, Y., Rangell, L., Reichelt, M. & O'Brien, T. Depletion of the
433 Central Metabolite NAD Leads to Oncosis-mediated Cell Death. *J. Biol. Chem.* **289**,

35182–92 (2014).

38. Dahmen, W., Webb, B. & Preiss, J. The Deamido-Diphosphopyridine Nucleotide and Diphosphopyridine Nucleotide Pyrophosphorylases of *Escherichia coli* and Yeast. *Arch. Biochem. Biophys.* **120**, 440–450 (1967).
39. Suhadolnik, R. J., Lennon, M. B., Uematsu, T., Monahan, J. E. & Baur, R. Role of adenine ring and adenine ribose of NAD⁺ in binding and catalysis with alcohol dehydrogenase, lactic dehydrogenase and glyceraldehyde-3-phosphate dehydrogenase. *J. Biol. Chem.* **252**, 4125–4133 (1977).
40. Schuber, F., Pascal, M. & Travo, P. Calf Spleen Nicotinamide Adenine Dinucleotide Glycohydrolase. Properties of the Active Site. *Eur. J. Biochem.* **83**, 205–214 (1978).
41. Xie, Y. F., MacDonald, J. F. & Jackson, M. F. TRPM2, calcium and neurodegenerative diseases. *International Journal of Physiology, Pathophysiology and Pharmacology* **2**, 95–103 (2010).
42. Fonfria, E. *et al.* TRPM2 is elevated in the tMCAO stroke model, transcriptionally regulated, and functionally expressed in C13 microglia. *J. Recept. Signal Transduct. Res.* **26**, 179–198 (2006).
43. Yang, K.-T. *et al.* Activation of the transient receptor potential M2 channel and poly(ADP-ribose) polymerase is involved in oxidative stress-induced cardiomyocyte death. *Cell Death Differ.* **13**, 1815–1826 (2006).

Figure legends for main text

Fig. 1 Few ADPR analogues with modifications in different parts of the molecule

activate TRPM2 in whole cell patch clamp experiments. Outward currents at a potential of

+15 mV were recorded as detailed in the Methods section. The pipette solutions contained

either no nucleotide (buffer), 100 $\mu\text{mol/L}$ ADPR or 100 $\mu\text{mol/L}$ of the indicated ADPR

analogue. 2-F-ADPR which showed a slightly increased current at 100 $\mu\text{mol/L}$ was tested

additionally at 300 $\mu\text{mol/L}$. Data for 30 $\mu\text{mol/L}$ 2'-deoxy-ADPR are from the same

experiment as Fig 2a. Currents from individual patch experiments are shown on logarithmic

scale as filled circles with the total number of experiments indicated. The median is indicated

by a bar. Since in some cases the number of data points was too small to test for normality,

data were analyzed by a nonparametric one-way ANOVA (Kruskal–Wallis test) followed by

comparison against buffer control, applying Dunn's correction for multiple testing. Results

significantly different from buffer control ($p < 0.05$) are indicated by an asterisk. Squaryl and

triazole compounds were dissolved in DMSO, the pipette solution contained 0.1% DMSO.

For buffer and ADPR control conditions DMSO was therefore included in the pipette solution

at the same final concentration. (ADPR - adenosine 5'-diphosphoribose; AMP - adenosine 5'-

monophosphate; ASqR - adenosine squaryl ribose; ATPR - adenosine 5'-triphosphate ribose;

IDPR - inosine-5'-diphosphoribose; Sal-AMS - salicyl-adenosine monosulfamide, 8-pCPT-

AMP - 8-(4-Chlorophenylthio)adenosine-5'-O-monophosphate; 8-Ph-ATrR - 8-Phenyl-

adenosine-1,4-triazole ribose). Abbreviations for ligands evaluated are consistent with those

in reference ¹³. Analogue structures shown are examples, see Supplementary Fig. 1-4 for all

structures.

Fig. 2 Modifications of the proximal ribose affect the ability of ADPR to activate TRPM2. **a**, Concentration response relationship for activation of TRPM2 by ADPR, 2'-deoxy-ADPR, 3'-deoxy-ADPR and 2'-Phospho-ADPR from HEK293 cells expressing hTRPM2. Free Ca^{2+} in the pipette solution was adjusted to 200 nmol/L. In the NMDG-based bath solution the I-V curve of TRPM2 showed characteristic reversal potential and outward rectification (Suppl. Fig. 5a). Maximum currents at +15mV are displayed as mean \pm SEM (n=6–12 for ADPR, 5–6 for 2'-Phospho-ADPR, 5–12 for 2'-deoxy-ADPR, 5–9 for 3'-deoxy-ADPR). **b**, Concentration response relationship for activation of endogenous TRPM2 in Jurkat cells. In the NaCl-based bath solution the current showed the reversal potential and I-V relationship expected for a non-selective cation channel (Suppl. Fig. 5b). Maximum inward currents at –80 mV are displayed as mean \pm SEM (n=2–13 for ADPR, 2–21 for 2'-deoxy-ADPR). Result from a single experiment with 250 $\mu\text{mol/L}$ 2'-deoxy ADPR in parenthesis (not included in the concentration response curve). The current axis is shown in reverse to facilitate comparison with panel a. **c**, Ca^{2+} -dependence of the concentration response relationship for ADPR and 2'-deoxy ADPR. Concentration response curves for ADPR (squares) and 2'-deoxy-ADPR (circles) with 50 nmol/L free Ca^{2+} in the pipette solution (dashed lines) are shown in addition to the curves with 200 nmol/L from panel a (solid lines). Maximum currents at +15mV are displayed as mean \pm SEM (at 50 nM Ca^{2+} n=2–6 for ADPR, 3–7 for 2'-deoxy-ADPR for 200 nM Ca^{2+} see panel a)

Fig. 3 Impact of 2'-deoxy-ADPR on hTRPM2 in excised inside-out patches. **a**, Current steps of hTRPM2 activated by 100 $\mu\text{mol/L}$ ADPR at different potentials. No activity was observed at 0 mV. **b**, I-V relationship from patches containing TRPM2 wt (filled symbols and solid lines) and TRPM2 T5L (open symbols and dashed lines) activated by either 100 $\mu\text{mol/L}$ ADPR (gray) or 2'-deoxy-ADPR (black) in the presence of 1 $\mu\text{mol/L}$ free Ca^{2+} (n=6-17

patches for TRPM2 wt and n=2–3 patches for TRPM2 T5L). **c**, Single channel slope conductance γ obtained by linear regression of the data in panel b. (unpaired, two-tailed T-tests of the mean \pm SEM obtained from linear regression, p values are indicated) **d**, Representative continuous recordings of excised inside out patches with the bath solution containing either 100 μ mol/L ADPR or 2'-deoxy-ADPR. **e-h, Quantitative analysis of continuous recordings from excised inside-out patches** **e**, Histograms of time to inactivation of wild type TRPM2 after activation by ADPR (light gray) or 2'-deoxy ADPR (dark gray) with exponential fit. **f**, Decay constants for the time to inactivation. (mean \pm SEM, extra sum-of-squares F-Test, p=0.0012). **g**, Average open probability after activation by ADPR (light gray) or 2'-deoxy-ADPR (dark gray). Whiskers indicate min and max, horizontal bar represents the median (Mann-Whitney test, p < 0.0001). **h**, Maximum number of simultaneously active channels in an excised patch after application of either ADPR (dark gray) or 2'-deoxy-ADPR (light gray). (mean \pm SEM, unpaired t-test, < 0.0001). **f-h** Number of recordings evaluated is indicated in the bars. Significant differences are indicated by asterisks.

Fig. 4 Human NMNAT-2 and CD38 synthesize 2'-deoxy-ADPR *in vitro*. **a**, β -nicotinamide 5'-mononucleotide (NMN) and 2'-deoxy-ATP were incubated with recombinant hNMNAT-2 and reaction products analyzed by HPLC. 2'-deoxy-AMP and 2'-deoxy-ADP were impurities contained in commercial 2'-deoxy-ATP. **b**, Saturation plot for ATP and 2'-deoxy-ATP as substrates of NMNAT-2. hNMNAT-2 was incubated with β -NMN and increasing concentrations of either ATP or 2'-deoxy-ATP. Initial reaction rate was calculated from the amount of product formed, determined by HPLC. Data for ATP were fitted to a Michaelis-Menten model. The data points up to 3 mmol/L 2'-deoxy-ATP looked sigmoidal and were thus fitted to a Hill model. At higher concentrations the reaction rate dropped rapidly,

indicating substrate inhibition (dashed line) Data are indicated as mean \pm SD (n=3, conditions with 3 mM and 9 mM 2'-deoxy-ATP n=6). **c**, Recombinant hCD38 hydrolyzes 2'-deoxy-NAD (from panel a) to yield the TRPM2 agonist 2'-deoxy-ADPR. **d**, CD38 activity was determined by incubation of Jurkat cells with 1,N⁶-etheno-NAD. Reaction velocity was calculated from the concentration of 1,N⁶-etheno-ADPR at different. CD38 activity on the cell surface was inhibited by araF-NAD. To obtain access to type III CD38 the plasma membrane was selectively permeabilized using saponin resulting in an increase in activity. After a second incubation with araF-NAD the activity was gone. For all conditions the number of experiments is indicated. For conditions tested in a one-way ANOVA for repeated measurements using Tukey's corrections for multiple testing the corrected p values are shown.

Fig. 5 The increase in 2'-deoxy-ADPR in Jurkat cells exposed to hydrogen peroxide depends on CD38. Wild type and CD38^{-/-} Jurkat cells were either exposed to 100 μ mol/L H₂O₂ for 5 min or left unstimulated. **a+d** Deproteinized extracts from these cells were separated by RP-HPLC and fractions co-eluting with authentic ADPR, NAD, 2'-deoxy-ADPR or 2'-deoxy-NAD were collected. **b+c+e+f** Fractions from the pre-fractionation were subjected to a second dimension of RP-HPLC. To correctly assign peaks, each sample was split and one half was spiked with the respective nucleotide (light gray lines). Representative chromatograms for each condition are shown. Since we could not achieve baseline separation for 2'-deoxy-ADPR, it was not analyzed quantitatively. The peak of 2'-deoxy-ADPR clearly increased in height when cells were exposed to hydrogen peroxide. In the chromatograms from CD38^{-/-} cells the respective peak is gone, regardless of stimulation. **g**, Quantitative analysis of the impact of H₂O₂ on intracellular 2'-deoxy-NAD. Independent experiments were initiated on 3 separate days over the course of one month, with each replication consisting of

multiple parallel experiments. 2–6 data points were obtained per experimental day. Results from single experiments are indicated as filled circles (horizontal bars indicate the mean) with the same shade of gray signifying individual experiments from a single day. Data are normally distributed in each group. Analysis by one-way ANOVA did not reveal significant differences for 2'-deoxy-NAD ($p=0.074$).

Fig. 6 Concentration of 2'-deoxy ADPR in Jurkat cells increases after exposure to hydrogen peroxide. **a**, Deproteinized cell extracts from either unstimulated Jurkat cells or Jurkat cells exposed to 100 $\mu\text{mol/L}$ H_2O_2 were applied to a Phenomenex Luna C8 column and a fraction co-eluting with chemically synthesized 2'-deoxy ADPR (R_t between 24 and 25 min) was collected **a + b**, The fractions were re-chromatographed on a Multohyp BDS-C18 5 μ column. To confirm identity of the peak co-eluting with 2'-deoxy ADPR, samples were also spiked with 15.6 nmol 2'-deoxy ADPR (2'-deoxy ADPR standard, light gray, is the same for panels **b + c** since data are from the same run). The slight enhancement of the spiked peak is in agreement with the amount of 2'-deoxy-ADPR added as spike (see standard trace for comparison). **d**, Quantitative analysis of the impact of H_2O_2 on intracellular 2'-deoxy ADPR (per 10^7 cells). Results from single experiments are indicated as gray symbols (horizontal bars indicating the median) with symbols of same shape and gray level signifying experiments from the same day. The number of independent preparations and the number of days (12 samples from 3 days for H_2O_2 stimulated cells vs 47 samples from 7 days for unstimulated cells) are indicated in the chart. Due to non-normal distribution, data were analyzed by a nonparametric Mann-Whitney test. P value is shown.

Online Methods

Chemical Synthesis and Purification of ADPR Analogues

Chemical synthesis, purification and characterization of 2'-deoxy-ADPR, 3'-deoxy-ADPR and all other non-commercial ADPR analogues, apart from hydroxyl-ethoxy-ethyl-ASq, was as described previously¹⁻³. Analogue identity was confirmed by ¹H-NMR and HRMS. Purity was checked by HPLC (>95%) and re-checked after storage.

Synthesis of hydroxyl-ethoxy-ethyl-ASq

3-(2-(2-hydroxyethoxy)ethylamino)-4-ethoxycyclobut-3-ene-1,2-dione

To a solution of 2-(2-aminoethoxy)ethanol (95 μ L, 0.951 mmol) and DIPEA (81 μ L, 0.467 mmol) in EtOH (8 mL) was added diethylsquarate (128 μ L, 0.865 mmol). After 1h, the solvent was removed under reduced pressure and the residue was purified on an Isco chromatographic system (DCM-acetone, 8:2 v/v) to yield the desired product as a colorless oil (165 mg, 91%). ¹H (400 MHz, *d*₄-MeOH) δ 4.79 (q, 2H, *J* = 7.1 Hz, OCH₂-Me), 3.85-3.61 (m, 8H, 4 x CH₂) and 1.51 (t, 3H, *J* = 7.1 Hz, CH₃). ¹³C (100 MHz, *d*₄-MeOH) δ 189.9 (C-2), 184.9 (C-1), 177.9 (C-3), 175.1 (C-4), 73.5, 70.9 (both CH₂), 70.7 (Et: CH₂), 62.2, 45.5 (both CH₂) and 16.2 (Et: CH₃). HRMS (ES⁺) calcd for C₁₀H₁₆NO₅ 230.1023 (MH)⁺ found 230.1031.

3-(2',3'-O-Isopropylidene-5'-amino-5'-deoxyadenosine)-4-(2-(2-hydroxyethoxy)ethyl-amino)cyclobut-3-ene-1,2-dione

To a solution of 3-(2-(2-hydroxyethoxy)ethylamino)-4-ethoxycyclobut-3-ene-1,2-dione (60 mg, 0.287 mmol) and DIPEA (27 μ L, 0.154 mmol) in EtOH-DMF (1:1 v/v, 1 mL) was added 2',3'-isopropylidene-5'-amino-5'-deoxyadenosine (96 mg, 0.315 mmol). After 26h, the solvent was removed under reduced pressure and the residue was purified on an Isco chromatographic system (DCM-MeOH, 8:2 v/v) to yield the desired product as a white foam (104 mg, 74%). ¹H (400 MHz, *d*₆-DMSO) δ 8.30 (s, 2H, H-8 and H-2), 6.24 (d, 1H, *J*_{1',2'} = 2.6 Hz, H-1'), 5.55

599 (dd, 1H, $J_{2',3'} = 6.4$ and $J_{2',1'} = 2.6$ Hz, H-2'), 5.16 (dd, 1H, $J_{3',2'} = 6.4$ and $J_{3',4'} = 3.7$ Hz, H-3'),
600 4.44-4.41 (m, 1H, H-4'), 4.07-4.04 (m, 1H, H-5'a), 3.94 (dd, 1H, $J_{5'b,5'a} = 14.1$ and $J_{5'b,4'} = 6.6$
601 Hz, H-5'b), 3.78 (brs, 2H, CH₂-O), 3.72-3.70 (br, 2H, CH₂-NH), 3.64 (brs, 2H, CH₂-O), 3.61-
602 3.59 (m, 2H, CH₂-OH), 1.65 (s, 3H, CH₃) and 1.44 (s, 3H, CH₃). ¹³C (100 MHz, *d*₆-DMSO) δ
603 184.2 (C-2), 183.3 (C-1), 169.6 (both C=C), 157.6 (C-6), 154.3 (C-2), 150.3 (C-4), 142.0 (C-
604 8), 120.7 (C), 115.9 (C-5), 91.5 (C-1'), 87.0 (C-4'), 85.1 (C-2'), 82.9 (C-3'), 73.6, 71.4, 62.1,
605 46.7 (all CH₂), 45.1 (C-5'), 27.6 and 25.6 (both CH₃). HRMS (ES⁺) calcd for C₂₁H₂₈N₇O₇
606 490.2045 (MH)⁺ found 490.2027.

607 *3-(5'-amino-5'-deoxyadenosine)-4-(2-(2-hydroxyethoxy)ethylamino)cyclobut-3-ene-1,2-dione*
608 **(23)**

609 *3-(2',3'-O-Isopropylidene-5'-amino-5'-deoxyadenosine)-4-(2-(2-hydroxyethoxy)ethylamino)-*
610 *cyclobut-3-ene-1,2-dione* (80 mg, 0.163 mmol) was stirred in a 75% aq. TFA solution (5 mL)
611 at rt for 1h. The solvents were evaporated under reduced pressure and the residue co-
612 evaporated with MeOH to remove any residual TFA. The remaining residue was purified on
613 an Isco purification system (DCM-MeOH, 8:2 v/v) to yield the desired compound as a white
614 solid (60 mg, 82%). ¹H (400 MHz, *d*₆-DMSO) δ 8.39 (s, 1H), 8.22 (s, 1H), 7.57 (br s, 2H),
615 7.37 (br s, 2H, NH₂), 5.97 (d, 1H, $J_{1',2'} = 5.8$ Hz, H-1'), 5.62 (d, $J = 6.1$ Hz, 2'-OH), 5.44 (d, J
616 = 4.8 Hz, 3'-OH), 4.75 (ddd, 1H, $J_{2',3'} = 6.4$, $J_{2',OH} = 6.1$, $J_{2',1'} = 5.8$ Hz, H-2'), 4.67 (t, $J = 5.3$,
617 OH), 4.21 (ddd, 1H, $J_{3',2'} = 6.4$, $J_{3',OH} = 4.8$, $J_{3',4'} = 4.0$ Hz, H-3'), 4.08-4.05 (m, 2H, H-4', H-
618 5'a), 3.85-3.80 (m, 1H, H-5'b), 3.69 (brs, 2H, CH₂-O), 3.56-3.49 (m, 6H, 3 × CH₂). ¹³C (125
619 MHz, *d*₆-DMSO) δ 182.6 (C-2), 182.4 (C-1), 167.8 (both C=C), 156.1 (C-6), 152.7 (C-2),
620 149.4 (C-4), 139.8 (C-8), 119.2 (C-5), 87.4 (C-1'), 83.6 (C-4'), 72.7 (C-2'), 72.1 (CH₂), 70.8
621 (C-3'), 70.0, 60.1 (both CH₂), 45.5 (C-5'), 43.2 (CH₂). HRMS (ES⁺) calcd for C₁₈H₂₄N₇O₇
622 450.1737 (MH)⁺ found 450.1730.

623

624 *Commercial ADPR Analogues*

625 2'-phospho-ADPR (**15**), 1,N⁶-etheno-ADPR (**12**), and 8-(4-Chlorophenylthio)adenosine-5'-
626 mono-phosphate (8-pCPT-AMP, **32**) were purchased from Biolog.

627 *Cell Culture*

628 Jurkat subclone JMP with high expression of CD3 was originally generated at University of
629 Erlangen, Medical Faculty, Erlangen, Germany. They were recently authenticated as Jurkat by
630 short tandem repeats (STR) profiling and tested negative for contamination with rodent cells
631 (DSMZ service for the authentication of human cell lines). Jurkat cells were cultured as
632 described before⁴. Briefly, cells were kept in RPMI-1640 with GlutaMax-I and 25 mM 4-(2-
633 hydroxyethyl)-1-piperazineethanesulfonic acid (HEPES) supplemented with 7.5% newborn
634 calf serum (FCS) and penicillin (100 units/mL)/streptomycin (100 µg/mL). Cell density was
635 kept between 0.3x10⁶ and 1.0x10⁶/mL. For determination of endogenous concentrations of 2'-
636 deoxy-ADPR which required large amounts of cells, Jurkat cells were cultivated in spinner
637 bottles at a cell density of up to 1.0x10⁶ cells/mL.

638 HEK293 Tet-On cells were obtained from Clontech/Takara. Wild type HEK293 cells were
639 kindly provided by Prof. Dr. Manfred Jücker (Department of Biochemistry and Signal
640 Transduction, University Medical Centre Hamburg-Eppendorf, Germany). HEK293 cells
641 were kept in DMEM medium with 4.5 g/L D-glucose and without pyruvate supplemented
642 with 10% fetal calf serum, 100 units/mL penicillin, and 100 µg/mL streptomycin. For
643 maintenance of HEK293 cell lines TRPM2#24 and EGFP#8 400 µg/mL G418-sulfate was
644 added to the medium. For the maintenance of HEK293 Tet-On cell line expressing the
645 TRPM2 T5L mutant medium was supplemented with 100 µg/mL G418 sulfate and 25 µg/mL
646 hygromycin B. All cells were kept at 37°C and 5% CO₂. HEK293 cells are a well-established
647 system for the electrophysiological characterization of recombinant ion channels. They

express very little endogenous ion channels that might confound measurements and patch clamp experiments are straightforward since cells tend to seal very well. To avoid the risk of using cross-contaminated cells the parental wild type HEK293 cells and the HEK293 Tet-On cell line expressing the T5L mutant of hTRPM2 were authenticated by STR profiling and tested negative for contamination with rodent cells (DSMZ service for the authentication of human cell lines). All cells were tested for mycoplasma contamination on a regular basis using an enzymatic assay (MycoAlert™ Mycoplasma Detection Kit, Lonza).

Generation of HEK293 Cell Lines

Generation of HEK293 cells with stable expression of hTRPM2 and EGFP (TRPM2 #24) has been described before¹. The complete open reading frame of wild type hTRPM2 was amplified from the expression vector pIRES2-EGFP-TRPM2 described previously⁴ using the primers 5'-GGAATTCCGCCACCATGGAGCCCTCAGCCCTG-3' and 5'-TACTGTCTGACTCAGTAGTGAGCCCC-3'. *EcoRI* and *SalI* sites in the primers allowed for integration of the amplicon into the respective sites of the multiple cloning site of pTRE-tight (Clontech/Takara). The mutation T5L described by Tóth and coworkers⁵ was introduced by QuikChange mutagenesis (Stratagene/Agilent) using the primers 5'-GGCCAGATCCCGCTGGACGAGATCGACGGTGTGAACTTC-3' and 5'-GAAGTTCACACCGTCGACTCGTCCAGCCGGGATCTGGCC-3'. The complete open reading frame was confirmed by DNA sequencing (MWG Eurofins). HEK 293 Tet-On cells (Clontech/Takara) were co-transfected with pTRE-tight-TRPM2 T5L and pTK-Hyg (Clontech/Takara). Transfectants were selected by adding 25 µg/mL hygromycin B to the culture medium. Clonal cell lines for further analysis were generated from surviving cells by limiting dilution and chosen according to their response to hydrogen peroxide as described before¹. While two clones showed a calcium signal in response to hydrogen peroxide, neither was inducible by doxycycline. Excised inside/out patches from both clones showed ADPR

inducible currents with a higher single channel conductance than wild type TRPM2 as was expected for the T5L mutant.

Whole Cell Patch Clamp Analysis of TRPM2 Activation

Whole cell patch clamp experiments were performed as described previously^{1,6}. Briefly, HEK293 cells with stable expression of human TRPM2 were seeded to 35 mm dishes. The day after medium was removed and replaced by bath solution (140 mM N-methyl-D-glucamine (NMDG), 5 mM KCl, 3.3 mM MgCl₂, 1 mM CaCl₂, 5 mM D-glucose, 10 mM HEPES, pH 7.4 adjusted with HCl). Patch pipettes with a resistance of 1.5 to 3.5 MΩ were pulled from thin-walled 1.5 mm diameter borosilicate (1.10 mm x 1.50 mm x 80 mm) glass capillaries and filled with pipette solution (120 mM KCl, 8 mM NaCl, 1 mM MgCl₂, 10 mM HEPES, 10 mM ethylene glycol-bis(β-aminoethyl ether)-N,N,N',N'-tetraacetic acid (EGTA), the concentration of free Ca²⁺ ions in the pipette solution was buffered to 50 nM or 200 nM by addition of either 2.3 mM or 5.6 mM CaCl₂ as calculated by Maxchelator: <http://maxchelator.stanford.edu/CaEGTA-NIST.htm>). Currents were compensated for fast and slow capacity transients and recorded using an EPC10 amplifier and PatchMaster software (HEKA Elektronik). Series resistance was compensated by 70%. Voltage ramps from -85 mV to +20 mV in 140 ms were applied every 5 s over a period of 450 s starting from a holding potential of -50 mV. For analysis the maximum outward current at +15 mV during the course of experiment was extracted from all experiments. In the NMDG-based bath solution the I-V curve of TRPM2 showed characteristic reversal potential and outward rectification (Supplementary Results, Supplementary Fig. 5a), facilitating differentiation between activation of the non-selective cation channel and leaky cells/patches. If the patch ruptured before peak current was obtained or if significant changes in series resistance occurred during the measurement, recordings were excluded from analysis.

Jurkat cells were seeded to 35 mm dishes coated with poly-L-Lysine (MW 70–150kDa, Sigma Aldrich). After cells had adhered to the dish, medium was removed and replaced by bath solution (140 mM NaCl, 2 mM MgCl₂, 2 mM CaCl₂, 5 mM KCl, 10 mM HEPES, and 5 mM glucose adjusted to pH 7.4 with NaOH). Pipettes were prepared as described above and filled with pipette solution (140 mM KCl, 2 mM MgCl₂, 2.5 mM EGTA, and 10 mM HEPES adjusted to pH 7.4 with KOH, the concentration of free Ca²⁺ ions in the solution was buffered to 50 nM by addition of 0.59 mM CaCl₂ as calculated by MaxChelator). Currents were recorded as described above. Voltage ramps from –85 mV to +65 mV in 200 ms were applied every 10 s over a period of 300 s starting from a holding potential of -60 mV.

Electrophysiological Recordings from Excised Inside/Out-Patches

Cells with stable expression of either wild type hTRPM2 or hTRPM2 T5L were seeded to 35 mm dishes 24–48 h before use. Before the experiments medium was exchanged for a buffer based on sodium gluconate (140 mmol/L Na gluconate, 2 mmol/L MgCl₂, 7.6 mmol/L CaCl₂, 10 mmol/L EGTA, 10 mM HEPES pH7.2, free Ca²⁺ concentration 1 μmol/L). Patch pipettes with resistances of 10–15 MΩ were pulled from thick-walled borosilicate glass capillaries (0.86 mm x 1.50 mm x 80 mm) using a Sutter P-97 and filled with the same solution (symmetrical solutions). 100 nmol/L Tetrodotoxin (TTX) was added to the pipette solution to block endogenous voltage-gated sodium channels⁷. For activation of the channel either ADPR or 2'-deoxy-ADPR was added to the bath solution. After excision of a patch with one or a few channels the fast capacity transients were compensated. For the determination of the average open probability the patch membrane was held at a potential of –60 mV and the current was continuously recorded for a maximum of 30 min. For the determination of the slope conductance the potential across the patch membrane was increased by 20 mV steps every 20 s starting from –60 mV with a delay of 100 ms between steps. Data were sampled at 10 kHz and recorded to disk using the EPC10 amplifier and

PatchMaster software (v2.32, HEKA Elektronik). For analysis of the single channel data recordings were filtered to remove 50 Hz mains hum by an electrical interference filter and low-pass-filtered (1 kHz) to remove high-frequency noise. To determine single channel conductance Gaussian distributions were fitted to current histograms of the recordings and voltage steps were calculated as difference between the centers of the distributions. To determine average open probabilities continuous recordings were filtered and base-line corrected and exported to a script for trapezoid integration of the area under the curve written in Python (www.python.org, v2.7) and using the numpy/scipy libraries (www.scipy.org , numpy v1.8.1 and scipy v0.12.0) for numerical computations. At points of permanent inactivation of channels the recording was split into sections and the sections were separately integrated. The resulting integrals were divided by number of channels, duration and average height of voltage steps at –60 mV. The number of simultaneously open channels in a patch (Fig 3h) was determined either from the steps in the recording or for recordings where identification of individual states was not possible the number of channels was calculated by dividing peak current by single channel current for –60 mV. For display purposes (Fig 3a+d) data was filtered with a 100 Hz low pass filter and down-sampled by a factor of 10.

Production of Recombinant Human CD38

A fragment of the open reading frame of human CD38 encoding amino acids P44 to I300 was amplified using the primers 5'-ATGGTACGTCTCAGGCCCCGAGGTGGCGCCAGCAGTG-3' and 5'-ATGGTACGTCTCAGCGCTGATCTCAGATGTGCAAGATGAATC-3'. The amplicon was digested with *Esp3I* and inserted into the *BsaI* site of the multiple cloning site of the eukaryotic expression vector pEXPR-iba42 (Iba). The resulting reading frame encodes an *N*-terminal BM40 signal sequence followed by a 6xHis-Tag, the extracellular part of CD38 and a C-terminal Strep-Tag. This open reading frame was confirmed by DNA sequencing (MWG

747 Eurofins). HEK293 cells were transfected with the expression vector and transfectants were
748 selected by addition of 400 µg/mL G418-sulfate to the culture medium. The bulk of surviving
749 cells was continuously kept as described above and the supernatant medium was collected
750 each time cells were sub-cultured. Soluble recombinant CD38 secreted by the cells was
751 purified from the pooled supernatant by affinity chromatography using Ni-NTA agarose
752 (Qiagen). Imidazole was removed from elution fractions by dialysis and the protein solution
753 concentrated by ultrafiltration.

754 *Enzymatic Synthesis of 2'-deoxy-NAD*

755 5 mmol/L β-NMN and 5 mmol/L 2'-deoxy ATP were incubated at 37°C with 1 µg/mL
756 recombinant human NMNAT-2 (R&D Systems) overnight. The enzyme was removed
757 afterwards by passing the sample through a centrifugal filter device with 10 kDa cutoff. The
758 sample volume was reduced using a SpeedVac evaporator. Separation of the product 2'-
759 deoxy-NAD from byproducts and remaining substrates was achieved by HPLC using a
760 250 mm×10 mm Luna C8 5 µm column (Phenomenex) equipped with a 10 mm×10 mm guard
761 cartridge containing a C8 ODS filter element (Phenomenex) at a flow rate of 2.5 mL/min with
762 the buffer (50 mmol/L ammonium acetate, 0.05% acetic acid, pH 5.4) containing increasing
763 amounts of methanol as outlined below. The fraction co-eluting with chemically synthesized
764 2'-deoxy-NAD was collected, dried using a SpeedVac evaporator, reconstituted in water and
765 checked for purity by HPLC as outlined below. Concentration of the solution was adjusted
766 against chemically synthesized 2'-deoxy-NAD.

767 *HPLC-based Enzyme Assays for NMNAT-2 and CD38*

768 Recombinant human NMNAT-2 (R&D Systems) at a concentration of 5 ng/µL was incubated
769 for 15 min at 37°C with 290µmol/L β-NMN and 2.5 mmol/L 2'-deoxy-ATP in assay buffer
770 (50 mmol/L Tris, 10 mmol/L MgCl₂, pH 7.6). Afterwards the enzyme was removed by
771 passing the samples through centrifugal filter devices with 10 kDa cutoff. Reaction products

were analyzed via reversed-phase ion pair (RP)-HPLC on a Multohyp BDS-C18 5 μ column (250 mm x 4.6 mm, particle size 5 μ m, CS Chromatographie Service) equipped with a security guard cartridge (4 mm x 3.0 mm) containing a C18 ODS filter element (Phenomenex) at a flow rate of 0.8 mL/min with the buffer (20 mmol/L KH₂PO₄, 5 mmol/L tetrabutylammonium dihydrogen phosphate, pH 6) containing increasing amounts of methanol. The methanol gradient was: 0 min (15%), 3.5 min (15%), 11 min (31.25%), 15 min (31.25%), 25 min (50%), 27 min (50%), 29 min (15%) and 38 min (15%). The DAD (Diode-Array detector, Agilent Technologies) was set to 260 nm for detection of nucleotides. Peak integration was performed using ChemStation Software (Rev. C.01.05, Agilent Technologies).

Peaks co-eluting with chemically synthesized 2'-deoxy-NAD were collected and methanol was removed on a SpeedVac evaporator. Afterwards pH was adjusted to 7.2 and the MgCl₂ concentration to 1 mmol/L. Part of the sample was incubated for 1 h at 37°C with 0.33 Units/mL nucleotide pyrophosphatase from *Crotalus adamanteus*. The remainder of the sample was incubated with a recombinant soluble form of human CD38 for 15 min at 37°C. The putative 2'-deoxy-ADPR peak from the CD38 reaction was collected for pyrophosphatase digest. In all cases the products were analyzed via reversed-phase ion pair HPLC as described above.

Substrate saturation plots

To create substrate saturation plots of human NMNAT-2 for the substrates ATP and 2'-deoxy-ATP, 30 ng recombinant NMNAT-2 (R&D Systems) was incubated in 100 μ l reaction buffer (25 mmol/L KH₂PO₄, 5 mmol/L DTT, 20 mmol/L MgCl₂, 0.5 mg/ml bovine serum albumin (BSA), adjusted to pH 7.5 with KOH) with different concentrations of the substrates (ATP, 2'-deoxy-ATP). For soluble recombinant human CD38, 0.5 ng or 1.0 ng of the enzyme

(produced as described above) was incubated in 100 µl reaction buffer (110 mmol/L KCl, 5 mmol/L KH₂PO₄, 10 mmol/L NaCl, 2 mmol/L MgCl₂, 20 mmol/L HEPES, pH 7.2 mit KOH) with different concentrations of either NAD or 2'-deoxy-NAD as substrate for 20 min at 37°C. Reactions were stopped by cooling the samples rapidly to nearly 0°C and removing the enzyme by centrifugation through a 10 kDa filter device (VivaSpin, Sartorius) at 4°C. The amount of product formed was determined by HPLC analysis as described above using external standards for quantification. In case of CD38 substrate solutions contained minor contaminations of either ADPR / 2'-deoxy-ADPR that were subtracted before kinetic parameters for the enzyme/substrate pairs were calculated using GraphPad Prism (v6.03, GraphPad Software).

Immunoprecipitation and western blot analysis of poly-ADP-ribosylated proteins

HEK-293 cells were seeded to 150 mm dishes. Four days later at 80-90% confluence medium was replaced by pre-warmed buffer (15 mmol/L HEPES, 140 mmol/L NaCl, 5 mmol/L KCl, 1 mmol/L MgCl₂, 10 mmol/L Glucose, 1.8 mmol/L CaCl₂, pH 7.4) and hydrogen peroxide was added to a final concentration of 1 mmol/L. After 5 min buffer was replaced by pre-warmed phosphate buffered saline (137.93 mmol/L NaCl, 2.67 mmol/L KCl, 8.06 mmol/L Na₂HPO₄, 1.47 mmol/L KH₂PO₄, 0.493 mmol/L MgCl₂, 0.901 mmol/L CaCl₂, pH 7.38) and cells were washed twice. Lysis of cells and isolation of poly ADP-ribosylated proteins was based on Gagné et al⁸. Dishes were put on ice and 2 mL lysis buffer (40 mmol/L HEPES, 120 mmol/L NaCl, 1 mmol/L EDTA, 0.3% CHAPS (w/v), pH 7.5) with protease inhibitor (Roche complete, EDTA-free) and PARG inhibitor ADP-HPD (Enzo Life Sciences) was added to the cells which then were detached from the dishes and kept on ice for 15 min and on overhead rotation at 4°C for an additional 20 min. Non-lysed cells were removed by centrifugation. Paramagnetic beads were washed twice with sodium acetate buffer (0.1 mol/L Na acetate, pH 5.0) and incubated 30 min at 4°C with either anti-pADPR antibody (10H,

Abcam # ab14459) or mouse normal IgG (Thermo Fisher Scientific) in PBS-T (PBS, 0.02% Tween20 (v/v)) on overhead rotation. Non-specific binding was prevented by incubation with blocking buffer for 1 h at room temperature. Directly before addition to the lysed cells beads were washed with lysis buffer with protease inhibitor. Beads were incubated with the cell lysate for 2 h at 4°C on overhead rotation and washed five times with lysis buffer. For Western blot analysis poly-ADP-ribosylated proteins were eluted from the beads by incubation in sample buffer (0.22 mol/L Tris, 22.6% (v/v) glycerol, 4% (w/v) SDS, 5.3% (v/v) 2-mercapto ethanol, pH6.8) at 65°C for 5 min. Afterwards proteins were separated by 10% SDS-PAGE and transferred to a PVDF membrane (Merck, Darmstadt) by tank blotting. The membrane was blocked in TBS-MT (50 mmol/L Tris, 150 mmol/L NaCl, pH 7.6, 0.1% Tween20 (v/v), 5% dry milk protein(w/v)) and incubated overnight at 4°C with the primary anti-PAR antibody (pADPR antibody from rabbit, R&D Systems/Bio-Techne #4336-APC-050) diluted 1:1000 in TBS-MT. The secondary goat anti-rabbit antibody conjugated to horseradish peroxidase (HRP) (Dianova #111-035-045) was applied in 1:10 000 dilution in TBS-MT. HRP was detected by chemoluminescence using an Image Quant LAS4000/LAS3000 (GE Healthcare Life Sciences) after incubation of the membrane in SuperSignal Working Solution (Thermo Fisher Scientific) for 5 min.

PARG hydrolysis of poly-ADP-ribosylated proteins and HPLC analysis of products

Beads with poly-ADP ribosylated proteins were washed in phosphate buffer (20 mmol/L KH₂PO₄, pH 7.2), resuspended in 100 µl phosphate buffer + 10 mmol/L MgCl₂ and after addition of 100 ng recombinant human PARG (Adipogen International) incubated for 2.5 h at 37°C. After removal of beads and PARG by passing the samples through centrifugal filter devices with 10kD cutoff, 1 µL citric acid, 1 µL chloroacetaldehyde and 33 µL water were added to 85 µL of the sample and incubated for 40 min at 80°C resulting in conversion of the adenine nucleotides to the respective fluorescent 1, N⁶-etheno compounds. Analysis of the

converted nucleotides was based on the method described by Bobalova et al.⁹ HPLC analysis was performed on either a 1200 Series system or a 1260 Infinity system (both Agilent Technologies) using a 250 mm×4.6 mm Multohyp BDS-C18 5μ column (CS Chromatographie Service) equipped with a 4.0mm×3.0mm guard cartridge containing a C18 ODS filter element (Phenomenex) at a flow rate of 0.8 mL/min with the buffer (100 mmol/L KH₂PO₄, pH 6) containing increasing amounts of methanol. The gradient was: 0 min (0% methanol), 22.5 min (35% methanol), 25 min (35% methanol), 29 min (0% methanol) and 38 min (0% methanol). Fluorescence of 1, *N*⁶-ethenoadenosine was detected at an emission wavelength of 410 nm after excitation at 230 nm. Peaks were integrated using ChemStation Software (Rev. C.01.05) from Agilent Technologies. Quantification was performed using external standards.

Assay for type III CD38 activity using permeabilized cells

10⁶ wildtype Jurkat cells or CD38^{-/-} Jurkat cells were washed, resuspended in 200 μl reaction buffer (140 mmol/L NaCl, 5 mmol/L KCl, 1 mmol/L NaH₂PO₄, 1 mmol/L MgSO₄, 1 mmol/L CaCl₂, 5.5 mmol/L Glucose, 20 mmol/L HEPES, pH7.4 with NaOH) and incubated with 1, *N*⁶-etheno-NAD at a final concentration of 50 μmol/L. Reaction was stopped after 0, 5, 10, 15 and 30 min by spinning down the cells and passing the supernatant through a centrifugal filter device with 10kD cutoff. Samples were analysed by HPLC using fluorescence detection as described below, to determine the amount of 1, *N*⁶-etheno-ADPR formed. Reaction rates were calculated from the increase in product by linear regression. To block the activity of CD38 on the cell surface, cells were incubated in 1 μmol/L araF-NAD in reaction buffer for either 40 min or 90 min at RT. Excess araF-NAD was removed by washing the cells in reaction buffer prior to the determination of the CD38 activity. To selectively permeabilize the plasma membrane 10⁶ cells were washed once in intracellular buffer (120 mmol/L KCl, 10 mmol/L NaCl, 1.2 mmol/L MgCl₂, 0.533 mmol/L CaCl₂, 10 mmol/L HEPES, 1 mmol/L EGTA, pH7.2

with KOH) and resuspended in intracellular buffer with 90 µg/mL saponin. After incubation at 37°C for 5 min cells were washed in nominally Ca²⁺ free intracellular buffer (120 mmol/L KCl, 10 mmol/L NaCl, 1.2 mmol/L MgCl₂, 10 mmol/L HEPES, pH7.2 with KOH) twice before CD38 activity was determined using 1, N⁶-etheno-NAD as described above. To test whether residual activity was due to CD38, permeabilized cells were also incubated with 1 µmol/L araF-NAD for 40 min at RT. Excess araF-NAD was removed by washing the cells prior to the determination of the CD38 activity as described above.

Quantification of endogenous 2'-deoxy-ADPR by HPLC

1x10⁸ Jurkat cells at a cell density of 1x10⁶ cells/mL were harvested from suspension, washed twice in Ca²⁺ measurement buffer (140 mmol/L, NaCl, 5 mmol/L KCl, 1 mmol/L MgSO₄, 1 mmol/L CaCl₂, 1 mmol/L NaH₂PO₄, 5.5 mmol/L D-glucose and 20 mmol/L HEPES, pH 7.4) and resuspended in 5 mL of the same buffer. After 25 min at 25°C hydrogen peroxide was added to a final concentration of 100 µmol/L. An additional 2 or 5 minutes later cells were collected by centrifugation and nucleotides extracted from the cells by addition of trichloroacetic acid, freeze/thawing and sonication. Denatured proteins and nucleic acids were removed by centrifugation and 25 pmol 1, N⁶-ethenoadenosine was added to the supernatant as internal standard. Trichloroacetic acid was removed by four cycles of extraction with diethyl ether. To remove residual diethyl ether samples were dried using a SpeedVac evaporator and reconstituted in water. After samples were filtered through 0.2 µm syringe filter devices, samples were again dried and reconstituted in 15% methanol/water. HPLC analysis was performed on either a 1200 Series system or a 1260 Infinity system (both Agilent Technologies). The first step of chromatographic separation was run on a 250 mm×10 mm Luna C8 5 µm column (Phenomenex) equipped with a 10 mm×10 mm guard cartridge containing a C8 ODS filter element (Phenomenex) at a flow rate of 2.5 mL/min with the

buffer (20 mmol/L KH₂PO₄, 5 mmol/L tetrabutylammonium dihydrogen phosphate, pH 6) containing increasing amounts of methanol. The gradient was: 0 min (15% methanol), 3.5 min (15% methanol), 11 min (31.25% methanol), 15 min (31.25% methanol), 25 min (50% methanol), 27 min (50% methanol) , and 29 min (15% methanol). Adenine nucleotides were detected using the DAD (photo diode array detector) at 260 nm. Fluorescence of 1, N⁶-ethenoadenosine was detected at an emission wavelength of 410 nm after excitation at 275 nm. Two fractions of roughly 2.5 mL were manually collected around the retention times of 1, N⁶-ethenoadenosine (R_t 13.5 min) and 2'-deoxy-ADPR (R_t 24.5 min). Fractions were dried on a SpeedVac evaporator and reconstituted in 15% methanol/water. After reconstitution samples were split into twin samples. For the 2'-deoxy-ADPR fractions one of the samples was spiked with 15.625 pmol 2'-deoxy-ADPR. The second step of chromatographic analysis was run on a 250 mm×4.6 mm Multohyp BDS-C18 5μ column (CS Chromatographie Service) equipped with a 4.0 mm×3.0 mm guard cartridge containing a C18 ODS filter element (Phenomenex) at a flow rate of 0.8 mL/min using the same buffer system and detection as above. The gradient was: 0 min (15% methanol), 3.5 min (15% methanol), 11 min (31.25% methanol), 15 min (31.25% methanol), 25 min (50% methanol), 27 min (50% methanol) , and 29 min (15% methanol). Peaks were integrated using ChemStation Software (Rev. C.01.05) from Agilent Technologies. Samples with peaks unsufficiently resolved for proper integration were excluded. Quantification was performed using external standards. Recovery was determined from the internal standard 1,N⁶-ethenoadenosine. Results for 2'-deoxy-ADPR were corrected for recovery.

HPLC of endogenous 2'-deoxy-ADPR and 2'-deoxy-NAD for HRMS and quantification of endogenous 2'-deoxy-NAD, NAD and ADPR

920 1×10^8 wild type Jurkat cells or CD38^{-/-} Jurkat cells per sample were prepared as described
921 above and either left unstimulated or stimulated for 5 min with 100 μ mol/L hydrogen
922 peroxide. After deproteination and extraction of the trichloroacetic acid by diethyl ether,
923 samples were dried on a SpeedVac evaporator to remove residual diethyl ether and
924 reconstituted in water. After samples were filtered through 0.2 μ m syringe filter devices,
925 samples were again dried on a SpeedVac evaporator and reconstituted in 3% methanol/water.
926 HPLC analysis was performed on either a 1200 Series system or a 1260 Infinity system (both
927 Agilent Technologies). The first step of chromatographic separation was run on a
928 250 mm \times 10 mm Luna C8 5 μ m column (Phenomenex) equipped with a 10 mm \times 10 mm guard
929 cartridge containing a C8 ODS filter element (Phenomenex) at a column temperature of 20°C
930 and a flow rate of 2.5 mL/min with the buffer (50 mmol/L ammonium acetate, 0.05% acetic
931 acid, pH 5.4) containing increasing amounts of methanol. The gradient was: 0 min
932 (3% methanol), 5 min (3% methanol), 35 min (50% methanol), 38 min (50% methanol), 45
933 min (3% methanol), and 50 min (3% methanol). Adenine nucleotides were detected as
934 described above. Five fractions of roughly 2.5 mL were manually collected around the
935 retention times of ADPR (R_t 8.2 min), NAD (R_t 12.9 min), 2'-deoxy-ADPR (R_t 13.9 min), 2'-
936 deoxy-NAD (R_t 16.5 min), and 1, *N*⁶-ethenoadenosine (R_t 24.5 min). All fractions were dried
937 on a SpeedVac evaporator. The fractions containing ADPR, NAD and 1, *N*⁶-ethenoadenosine
938 were reconstituted in buffer (20 mmol/L KH₂PO₄, 5 mmol/L tetrabutylammonium dihydrogen
939 phosphate, pH 6 containing 15% methanol) whereas the fractions containing 2'-deoxy-ADPR
940 and 2'-deoxy-NAD were reconstituted in 3% methanol/water. After reconstitution all samples
941 except the ones for 1, *N*⁶-ethenoadenosine were split into twin samples. One half of the twin
942 sample was spiked with an appropriate amount of the respective nucleotide (ADPR with 100
943 or 250 pmol, NAD with 5 nmol, 2'-deoxy-ADPR with 62.5 pmol and 2'-deoxy-NAD with
944 15.63 pmol). The samples with ADPR, NAD, and 1, *N*⁶-ethenoadenosine were run on a

Multohyp BDS-C18 5 μ column using the same (ion pair) conditions as described above. For the samples with 2'-deoxy-ADPR and 2'-deoxy-NAD which were to be submitted to HRMS the second step of chromatographic analysis was run on a 250 mm \times 4.6 mm Multohyp BDS-C18 5 μ column (CS Chromatographie Service) equipped with a 4.0 mm \times 3.0 mm guard cartridge containing a C18 ODS filter element (Phenomenex) at a column temperature of 25°C and a flow rate of 0.8 mL/min with the buffer (50 mmol/L ammonium acetate, 0.05% acetic acid, pH 5.4) containing increasing amounts of methanol. The gradient was: 0 min (3% methanol), 7 min (3% methanol), 32 min (50% methanol), 35 min (50% methanol), 41 min (3% methanol), and 45 min (3% methanol). Adenine nucleotides were detected as described above. Separate fractions of roughly 500 μ L were manually collected for 2'-deoxy-ADPR (R_t 10.85 min) and 2'-deoxy-NAD (R_t 17.2 min) around the retention times of the respective standards. Fractions were dried on a SpeedVac evaporator and submitted to HRMS. Quantification using external standards was done as described above. Recovery was determined from the internal standard 1, N^6 -ethenoadenosine. Since recovery was always around 100% results were not corrected during these experiments.

High resolution mass spectrometry(HRMS)

HRMS was carried out using ultrahigh resolution ESI-QTOF on a maXis HD Bruker Daltonics instrument in negative mode with direct injection (50 μ L). Spectra were acquired in full scan mode in the mass range 100 – 750 m/z and the baseline subtracted (MilliQ water).

Generation of CD38^{-/-} Jurkat cell line using CRISPR/Cas9

Knock-out of CD38 in Jurkat subclone JMP was performed by CRISPR/Cas9 using the expression plasmids pX330-Puro-T2A-hCas9 and pCAG-EGxxFP, which were kindly provided by Prof. Dr. Alexander Flügel (Department of Neuroimmunology, University Medical Center Göttingen, Göttingen, Germany). The sgRNA sequence (CCACCGCGAGCACCACGACG) was designed with the GenScript gRNA design tool

(<http://www.genscript.com/gRNA-design-tool.html>). The adapted expression plasmids were co-transfected into Jurkat cells by electroporation. EGFP positive cells from the transfection were sorted and individualized by FACS (FACS Sorting Core Unit, University Medical Centre Hamburg-Eppendorf, Germany). Resulting Jurkat clones were characterized regarding CD38 protein expression and NAD glycohydrolase activity.

Preparation of membrane fractions from Jurkat cells

Membrane fractions from Jurkat cells were prepared as described previously^{10,11}. Briefly, either 5×10^7 wild type Jurkat cells or CD38^{-/-} Jurkat cells were suspended in lysis buffer (110 mmol/L NaCl, 20 mmol/L HEPES, pH 7.4) with protease inhibitor mix (Roche) and disrupted using a dounce homogenizer. After removal of undisrupted cells and intact nuclei, membranes were enriched by centrifugation at 10 000xg. The membrane pellet was resuspended in lysis buffer and protein content determined by Bradford protein assay (Bio-Rad) against BSA as standard.

Assay of NAD glycohydrolase activity

NAD glycohydrolase activity in P10 membranes from wild type Jurkat cells or CD38^{-/-} Jurkat cells was determined as described previously^{10,11}. Briefly, 20 µg of P10 membrane proteins from wild type Jurkat cells or CD38^{-/-} Jurkat cells were incubated with 1, N⁶-etheno-NAD (100 µmol/L) in buffer (140 mmol/L, NaCl, 5 mmol/L KCl, 1 mmol/L MgSO₄, 1 mmol/L CaCl₂, 1 mmol/L NaH₂PO₄, 5.5 mmol/L D-glucose and 20 mmol/L HEPES, pH 7.4). In the course of the reaction fluorescence is increasing due to the higher fluorescence of the product 1, N⁶-etheno-ADPR compared to the substrate. The increase in fluorescence was followed (excitation at 300 nm, emission at 410 nm) using an Infinite M200 micro plate reader (Tecan). The amount of product formed was calculated from the fluorescence readings using a 1, N⁶-etheno-ADPR standard curve.

Western Blot analysis of CD38 activity

CD38 expression in Jurkat cells was analyzed as described recently^{10,11}. Briefly 60 µg of P10 membrane proteins from wild type and CD38^{-/-} Jurkat cells were separated on a 12% non-reducing SDS-PAGE (0.4% SDS) and subsequently transferred to a PVDF membrane (Immobilon-FL, Millipore). The membrane was probed with a primary antibody against human CD38 (1:200, mouse monoclonal antibody AT-1, Santa Cruz Biotechnology #sc-7325) and a secondary goat anti-mouse antibody conjugated to horse radish peroxidase (1:10 000, Santa Cruz Biotechnology #sc-2302). Incubation of the membrane in SuperSignal Working Solution (Thermo Fisher Scientific) for 5 min allowed for detection of the secondary antibody by chemiluminescence using an Image Quant LAS4000/LAS3000 (GE Healthcare Life Sciences).

Statistical Analysis

Statistical analysis was performed using GraphPad Prism (v 6.03, GraphPad Software). Quantitative data were tested for normality using D'Agostino-Pearson Omnibus Test ($\alpha=0.05$). If all groups were normally distributed, data is reported as mean±SEM (standard error of the mean) and parametric tests were used (unpaired, two-tailed T-test or one-way ANOVA). In case of non-normal distribution or if the sample size for groups was too small to test for normality, data is reported as median with interquartile range and non-parametric tests (Mann-Whitney test, Kruskal-Wallis test) were chosen. If non-normal data were to be compared against a hypothetical value (especially against 0) a Wilcoxon Signed Rank Test was used. Post-hoc tests were performed as Holm-Sidak or Dunn's test with p-values corrected for multiple testing.

Linear and non-linear regression analysis was performed using GraphPad Prism (v 6.03, GraphPad Software). For fitting of concentration-response curves (Fig. 2) a four parameter logistic model has been chosen. Conditions were: bottom value constrained to 0 and Hill

coefficient shared between data sets. For the analysis of channel inactivation (Fig. 3e+f) a histogram of the frequency distribution with a bin width of 5 s was generated and a one phase exponential decay function fitted to the data by non-linear regression. To test whether parameters of fit differ between conditions extra-sum-of-squares F tests were used. In case of the slope conductance (Fig. 3c) data were fitted to a linear equation (without intercept). To compare the slope conductance between channel variants and agonists the results from the linear regression (slope \pm SEM) were tested by multiple unpaired, two-tailed T-tests assuming normal distribution of the residuals and without correction for multiple testing.

An a priori power analysis to determine sample sizes has not been done. For all statistical tests a significance level α of 0.05 was adopted.

1030 **Methods-only references**

- 1031 1. Moreau, C. *et al.* Structure-activity relationship of adenosine 5'-diphosphoribose at the
 1032 transient receptor potential melastatin 2 (TRPM2) channel: Rational design of
 1033 antagonists. *J. Med. Chem.* **56**, 10079–10102 (2013).
- 1034 2. Zhang, B. *et al.* 2'-deoxy cyclic adenosine 5'-diphosphate ribose derivatives:
 1035 importance of the 2'-hydroxyl motif for the antagonistic activity of 8-substituted
 1036 cADPR derivatives. *J. Med. Chem.* **51**, 1623–36 (2008).
- 1037 3. Ashamu, G. A., Sethi, J. K., Galione, A. & Potter, B. V. Roles for adenosine ribose
 1038 hydroxyl groups in cyclic adenosine 5'-diphosphate ribose-mediated Ca²⁺ release.
 1039 *Biochemistry* **36**, 9509–17 (1997).
- 1040 4. Kirchberger, T. *et al.* 8-Bromo-cyclic inosine diphosphoribose: towards a selective
 1041 cyclic ADP-ribose agonist. *Biochem. J.* **422**, 139–149 (2009).
- 1042 5. Tóth, B. & Csanády, L. Pore collapse underlies irreversible inactivation of TRPM2
 1043 cation channel currents. *Proc. Natl. Acad. Sci. U. S. A.* **109**, 13440–13445 (2012).
- 1044 6. Partida-Sanchez, S. *et al.* Chemotaxis of mouse bone marrow neutrophils and dendritic
 1045 cells is controlled by adp-ribose, the major product generated by the CD38 enzyme
 1046 reaction. *J. Immunol.* **179**, 7827–7839 (2007).
- 1047 7. He, B. & Soderlund, D. M. Human embryonic kidney (HEK293) cells express
 1048 endogenous voltage-gated sodium currents and Na v 1.7 sodium channels. *Neurosci.*
 1049 *Lett.* **469**, 268–72 (2010).
- 1050 8. Gagné, J. P. *et al.* Quantitative proteomics profiling of the poly(ADP-ribose)-related
 1051 response to genotoxic stress. *Nucleic Acids Res.* **40**, 7788–7805 (2012).
- 1052 9. Bobalova, J., Bobal, P. & Mutafova-Yambolieva, V. N. High-performance liquid

1053 chromatographic technique for detection of a fluorescent analogue of ADP-ribose in
1054 isolated blood vessel preparations. *Anal. Biochem.* **305**, 269–276 (2002).

1055 10. Schmid, F., Fliegert, R., Westphal, T., Bauche, A. & Guse, A. H. Nicotinic Acid
1056 Adenine Dinucleotide Phosphate (NAADP) degradation by alkaline phosphatase. *J.*
1057 *Biol. Chem.* **287**, 32525–32534 (2012).

1058 11. Schmid, F., Bruhn, S., Weber, K., Mittrücker, H. W. & Guse, A. H. CD38: A NAADP
1059 degrading enzyme. *FEBS Lett.* **585**, 3544–3548 (2011).

1060
1061 **Statement on image integrity**

1062 The authors confirm that the paper complies with Nature Publishing policy concerning image
1063 integrity.

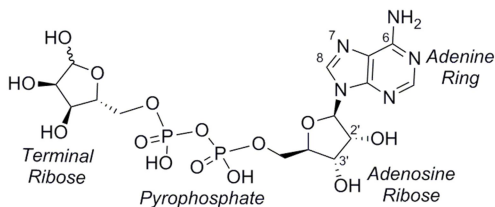
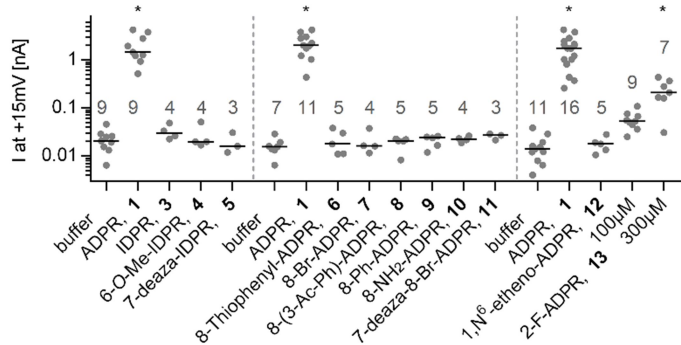
1064 **Statement on competing financial interests**

1065 The authors declare that they do not have any competing financial interests.

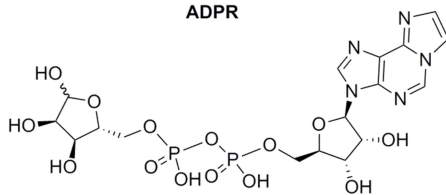
1066 **Data Availability Statement**

1067 Any materials, associated protocols, and other supporting data may be obtained from the
1068 corresponding author (guse@uke.de).

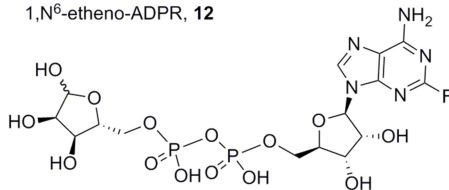
a Adenine Modifications



ADPR

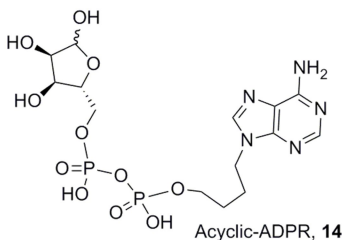
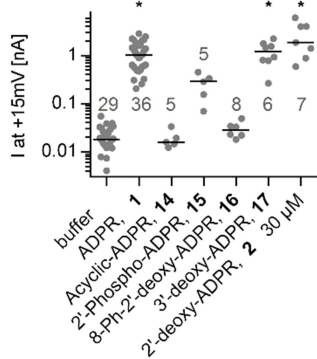


1,N⁶-etheno-ADPR, 12

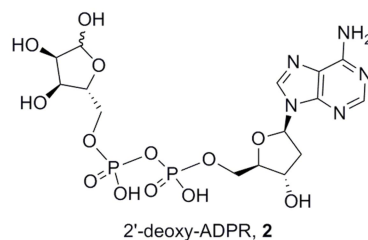


2-F-ADPR, 13

b Adenosine Ribose Modifications

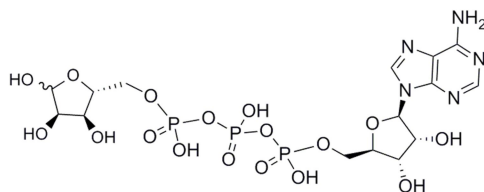
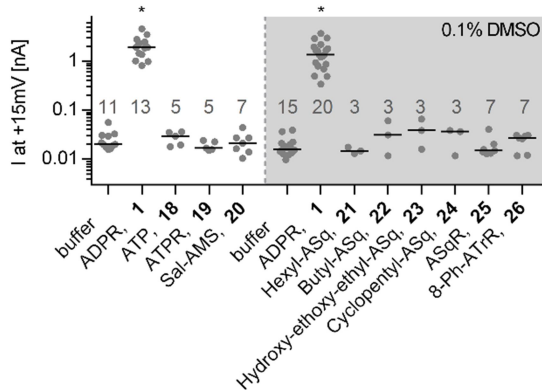


Acyclic-ADPR, 14

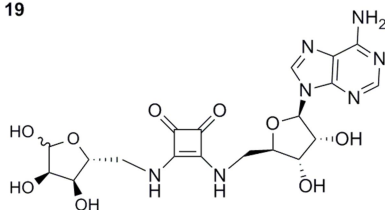


2'-deoxy-ADPR, 2

c Pyrophosphate Modifications

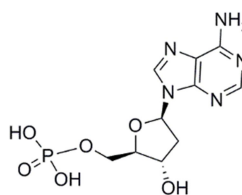
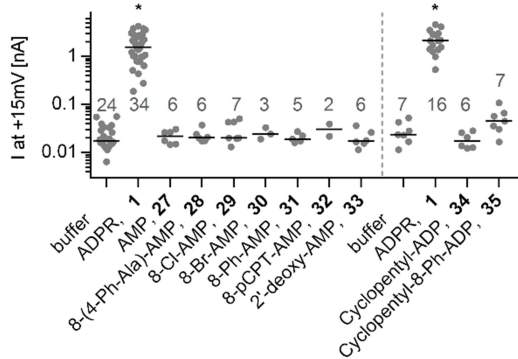


ATPR, 19

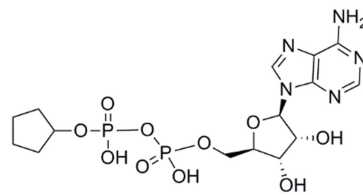


ASqR, 25

d Terminal Ribose Modifications



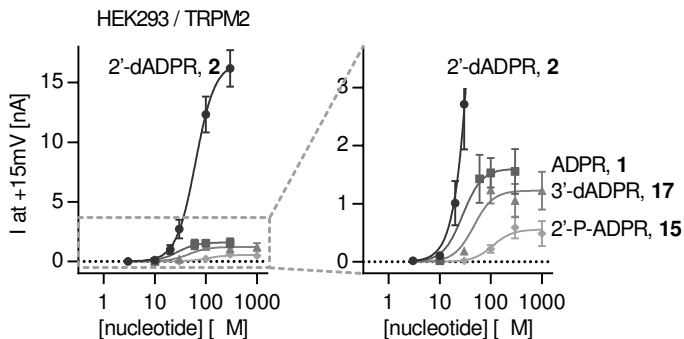
2'-deoxy-AMP, 33



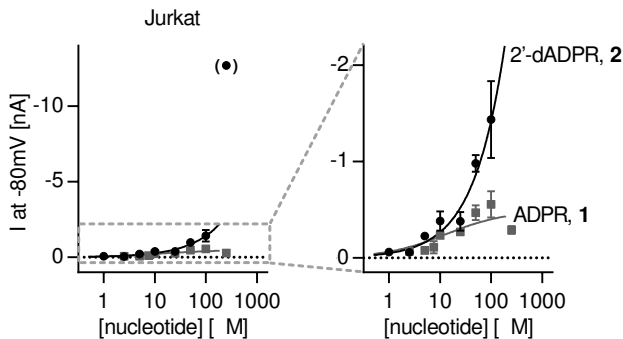
Cyclopentyl-ADP, 34

Figure 2

a



b



c

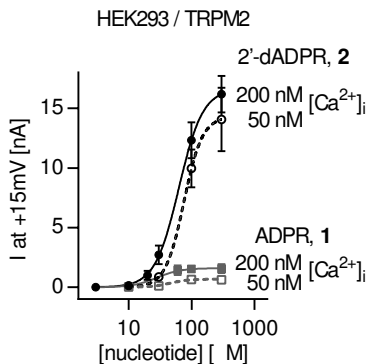


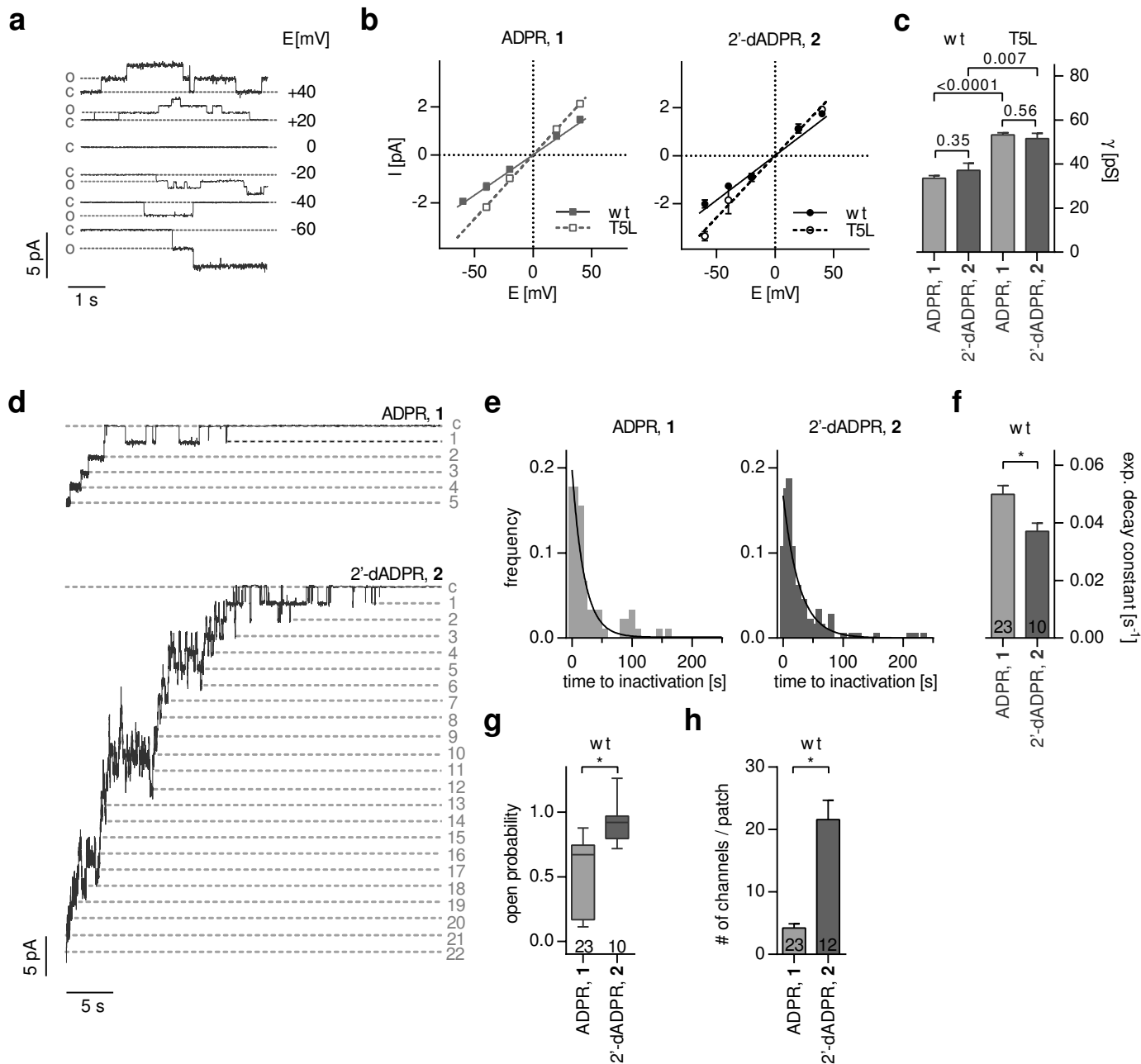
Figure 3

Figure 4

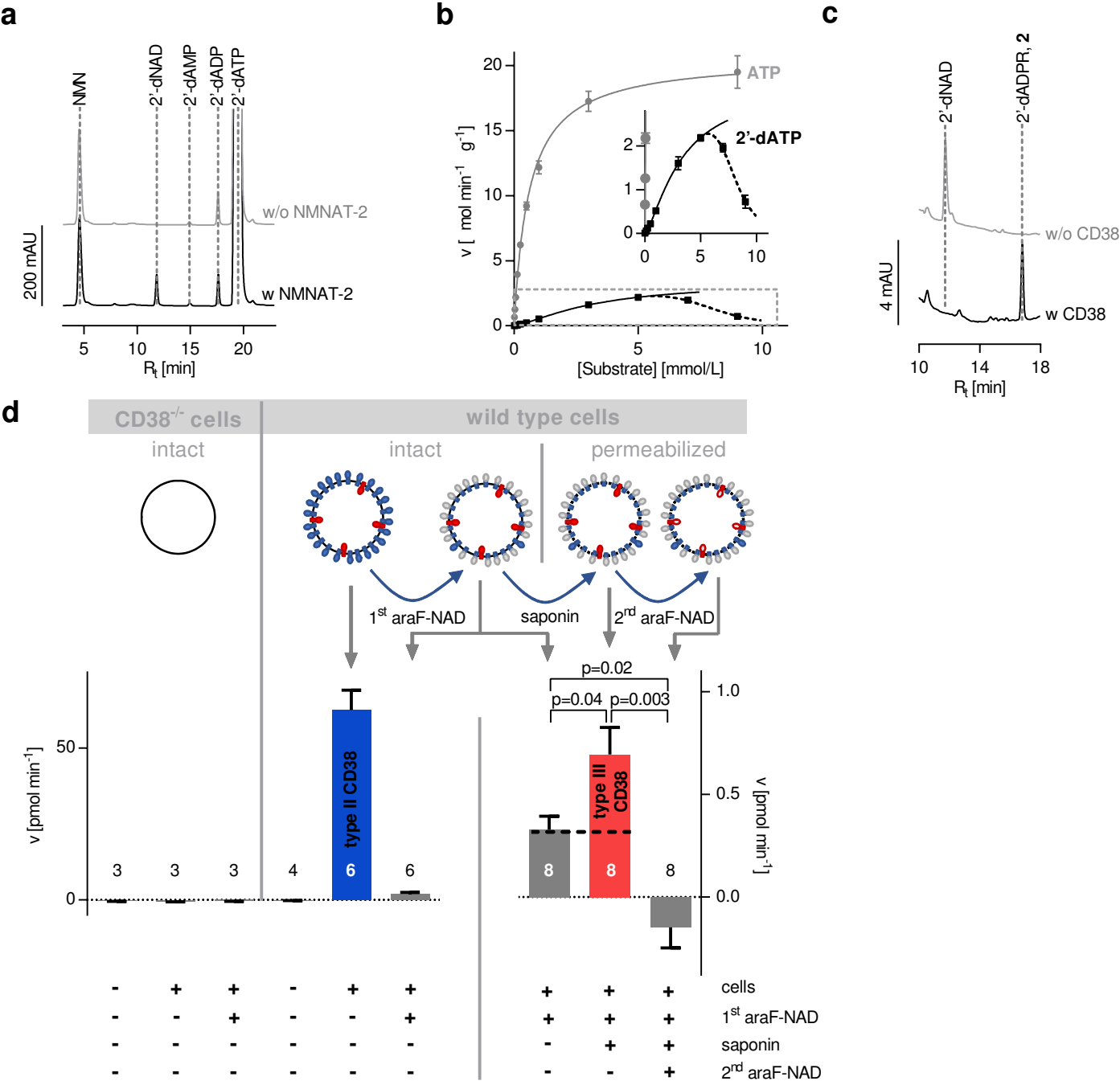


Figure 5

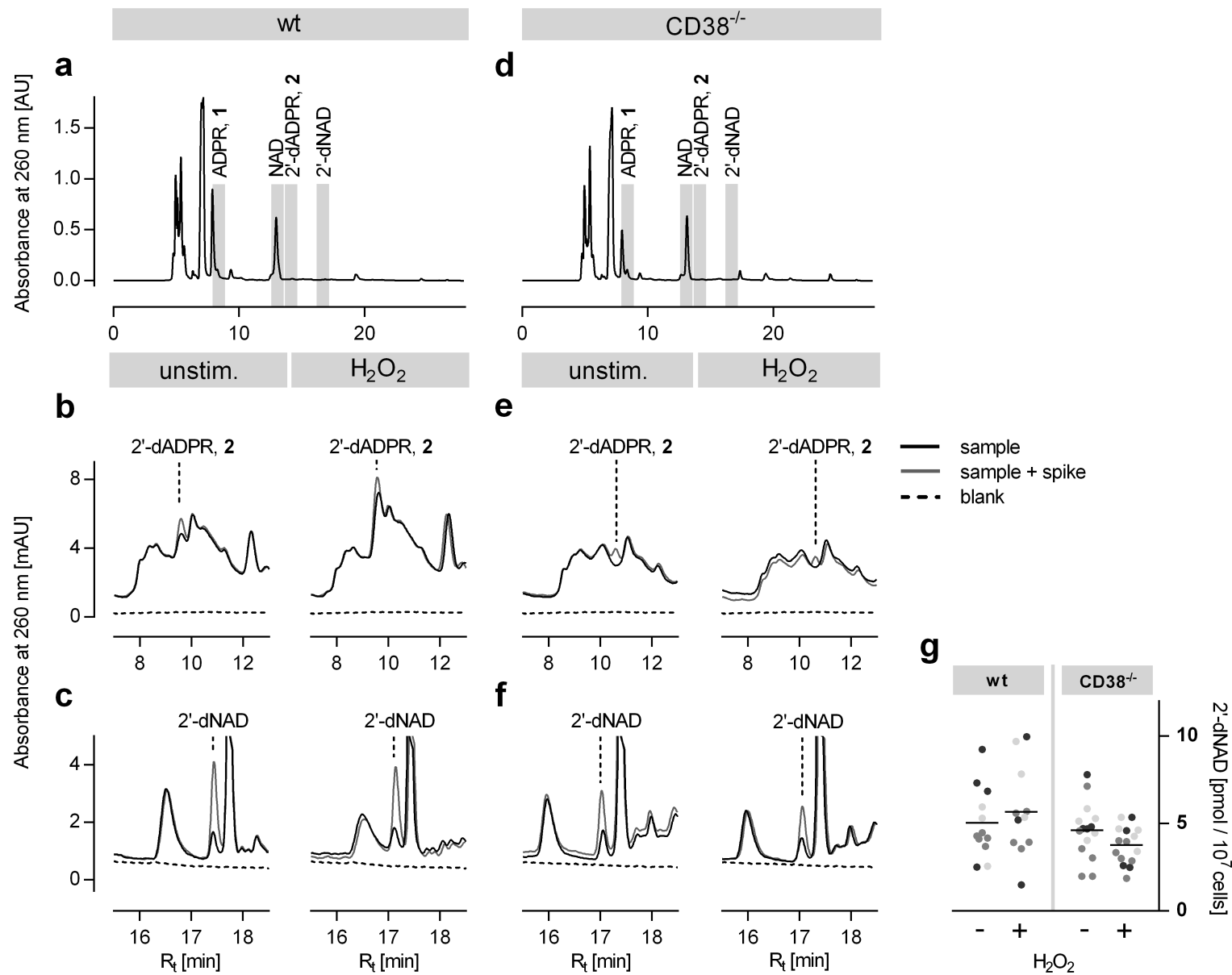
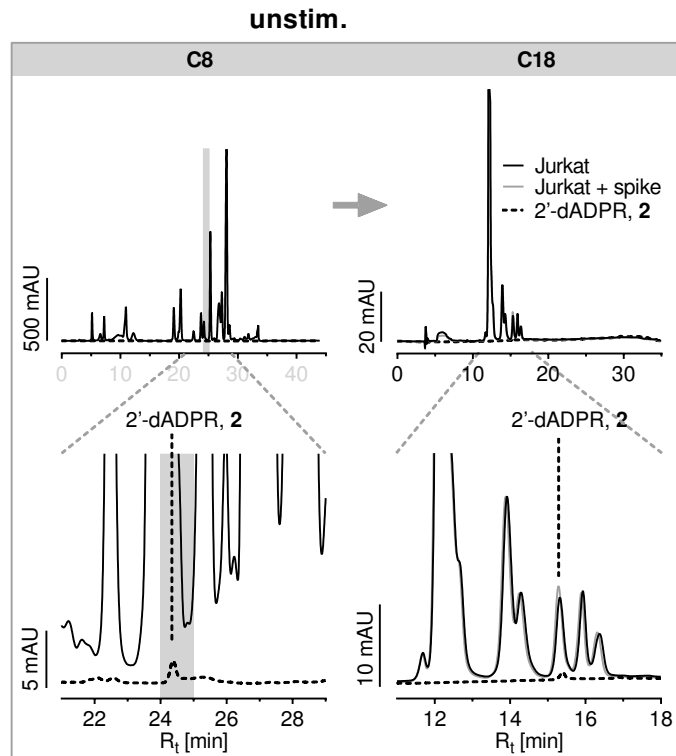
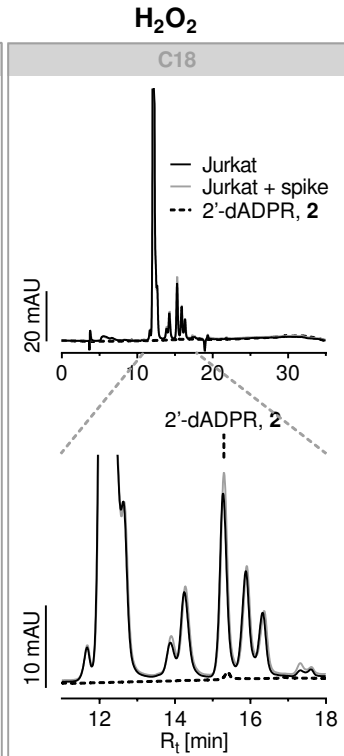


Figure 6

a



b



c

